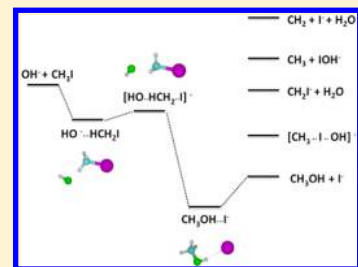


# Direct Dynamics Simulations of the Product Channels and Atomistic Mechanisms for the $\text{OH}^- + \text{CH}_3\text{I}$ Reaction. Comparison with Experiment

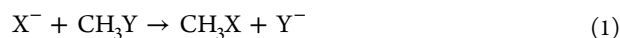
Jing Xie,<sup>†</sup> Rui Sun,<sup>†</sup> Matthew R. Siebert,<sup>‡</sup> Rico Otto,<sup>§</sup> Roland Wester,<sup>§</sup> and William L. Hase\*<sup>†</sup><sup>†</sup>Department of Chemistry and Biochemistry, Texas Tech University, Lubbock, Texas 79409-1061, United States<sup>‡</sup>Department of Chemistry, Missouri State University, Springfield, Missouri 65897, United States<sup>§</sup>Institut für Ionenphysik und Angewandte Physik, Universität Innsbruck, Technikerstraße 25/3, A-6020 Innsbruck, Austria

**ABSTRACT:** Electronic structure and direct dynamics calculations were used to study the potential energy surface and atomic-level dynamics for the  $\text{OH}^- + \text{CH}_3\text{I}$  reactions. The results are compared with crossed molecular beam, ion imaging experiments. The DFT/B97-1/ECP/d level of theory gives reaction energetics in good agreement with experiment and higher level calculations, and it was used for the direct dynamics simulations that were performed for reactant collision energies of 2.0, 1.0, 0.5, and 0.05 eV. Five different pathways are observed in the simulations, forming  $\text{CH}_3\text{OH} + \text{I}^-$ ,  $\text{CH}_2\text{I}^- + \text{H}_2\text{O}$ ,  $\text{CH}_2 + \text{I}^- + \text{H}_2\text{O}$ ,  $\text{IOH}^- + \text{CH}_3$ , and  $[\text{CH}_3\text{--I--OH}]^-$ . The  $\text{S}_{\text{N}}2$  first pathway and the proton-transfer second pathway dominate the reaction dynamics. Though the reaction energetics favor the  $\text{S}_{\text{N}}2$  pathway, the proton-transfer pathway is more important except for the lowest collision energy. The relative ion yield determined from the simulations is in overall good agreement with experiment. Both the  $\text{S}_{\text{N}}2$  and proton-transfer pathways occur via direct rebound, direct stripping, and indirect mechanisms. Except for the highest collision energy, 70–90% of the indirect reaction for the  $\text{S}_{\text{N}}2$  pathway occurs via formation of the hydrogen-bonded  $\text{OH}^- \cdots \text{HCH}_2\text{I}$  prereaction complex. For the proton-transfer pathway the indirect reaction is more complex with the roundabout mechanism and formation of the  $\text{OH}^- \cdots \text{HCH}_2\text{I}$  and  $\text{CH}_2\text{I}^- \cdots \text{HOH}$  complexes contributing to the reaction. The majority of the  $\text{S}_{\text{N}}2$  reaction is direct at 2.0, 1.0, and 0.5 eV, dominated by stripping. At 0.05 eV the two direct mechanisms and the indirect mechanisms have nearly equal contributions. The majority of the proton-transfer pathway is direct stripping at 2.0, 1.0, and 0.5 eV, but the majority of the reaction is indirect at 0.05 eV. The product relative translational energy distributions are in good agreement with experiment for both the  $\text{S}_{\text{N}}2$  and proton-transfer pathways. For both, direct reaction preferentially transfers the product energy to relative translation, whereas transfer to product vibration is more important for the indirect reactions. For the proton-transfer reactions the velocity scattering angle distribution is peaked in the forward direction and in quite good agreement with experiment. However, for the  $\text{S}_{\text{N}}2$  reaction, the experimental scattering is isotropic in nature whereas forward scattering dominates the simulation distributions. The implication is that the simulations give too much stripping, which leads to forward scattering. The dynamics for the  $\text{OH}^- + \text{CH}_3\text{I}$   $\text{S}_{\text{N}}2$  pathway are similar to those found previously for the  $\text{F}^- + \text{CH}_3\text{I}$   $\text{S}_{\text{N}}2$  reaction.



## I. INTRODUCTION

There is substantial interest in understanding the atomistic dynamics of  $\text{X}^- + \text{CH}_3\text{Y}$  ion–molecule reactions.<sup>1–7</sup> If X and Y are halogens, the dominant reaction mechanism is  $\text{S}_{\text{N}}2$  nucleophilic substitution,<sup>1,7</sup> i.e.



For the highly electronegative anion reactant  $\text{F}^-$ , proton transfer forming the  $\text{HF} + \text{CH}_2\text{Y}^-$  products also becomes an important pathway.<sup>8</sup> The traditional  $\text{S}_{\text{N}}2$  mechanism assumes  $\text{C}_{3v}$  symmetry with the reaction proceeding through long-lived  $\text{X}^- \cdots \text{CH}_3\text{Y}$  and  $\text{CH}_3\text{X} \cdots \text{Y}^-$  ion–dipole complexes with statistical unimolecular dynamics, which are separated by a  $[\text{X} \cdots \text{CH}_3 \cdots \text{Y}]^-$  central barrier.<sup>1–7</sup> Detailed studies, both experimental<sup>9–19</sup> and computational,<sup>20–28</sup> have shown there are substantial nonstatistical dynamics for the  $\text{S}_{\text{N}}2$  mechanism. The rate constant for the  $\text{X}^- + \text{CH}_3\text{Y} \rightarrow \text{X}^- \cdots \text{CH}_3\text{Y}$  association reaction is less than the ion–molecule capture rate constant as

a result of inefficient energy transfer from  $\text{X}^- + \text{CH}_3\text{Y}$  relative translation to  $\text{X}^- \cdots \text{CH}_3\text{Y}$  vibration/rotation.<sup>21,23</sup> The unimolecular dynamics of the  $\text{X}^- \cdots \text{CH}_3\text{Y}$  complex is nonstatistical and non-RRKM as a result of inefficient energy transfer between the intermolecular and intramolecular vibrational modes of the complex.<sup>9–12,14,16,21,23,25</sup> The presence of both intermolecular and intramolecular complexes in the reaction dynamics leads to important central barrier recrossings in the reaction dynamics.<sup>22,27</sup> For exothermic  $\text{S}_{\text{N}}2$  reactions, formation of the postreaction complex  $\text{CH}_3\text{X} \cdots \text{Y}^-$  is often unimportant.<sup>17–19,28</sup>

Formation of the  $\text{X}^- \cdots \text{CH}_3\text{Y}$  prereaction complex may not be important for the  $\text{S}_{\text{N}}2$  reaction. With excess reactant

**Special Issue:** Joel M. Bowman Festschrift

**Received:** January 23, 2013

**Revised:** March 18, 2013

**Published:** March 20, 2013



translational energy the reaction may proceed directly from reactants to products without complex formation.<sup>12,15,17,18,23,28</sup> Direct reaction is also found with excitation of the C–Y stretching vibration of the CH<sub>3</sub>Y reactant.<sup>20</sup> An indirect S<sub>N</sub>2 reaction without complex formation, named the “roundabout” mechanism, has been identified.<sup>17</sup> The reaction path for the S<sub>N</sub>2 reaction may not have C<sub>3v</sub> symmetry. For the F<sup>−</sup> + CH<sub>3</sub>I S<sub>N</sub>2 reaction there is a hydrogen-bonded F<sup>−</sup>---H–CH<sub>2</sub>I prereaction complex, which is connected to the products via the [F–H–CH<sub>2</sub>--I]<sup>−</sup> central barrier transition state that does not have C<sub>3v</sub> symmetry.<sup>29</sup> The F<sup>−</sup> + CH<sub>3</sub>OH reaction has a CH<sub>3</sub>OH--F<sup>−</sup> hydrogen-bonded postreaction complex.<sup>30</sup> The potential energy surface (PES) for the S<sub>N</sub>2 reaction may often be more complex than that depicted by the C<sub>3v</sub> model.<sup>6</sup>

In recent work Wester and co-workers have studied the OH<sup>−</sup> + CH<sub>3</sub>I reaction by molecular beam, ion-imaging experiments.<sup>19</sup> In these experiments, OH<sup>−</sup> anions were crossed with a neutral gas jet from a supersonic expansion at well-defined relative kinetic energies. The ions were buffer gas cooled in a radio frequency ion trap before they were injected into the interaction region. The ionic products from reactive collisions were then collected using a pulsed velocity map imaging spectrometer. The authors found multiple reaction products and reaction pathways, whose dynamics appear to be complex and not well described by statistical models. In a preliminary report,<sup>31</sup> we presented an incomplete direct dynamics simulation of the OH<sup>−</sup> + CH<sub>3</sub>I reaction dynamics. In this article a full report of a complete direct dynamics simulation is given, which includes: a description of the PES and atomistic pathways for the different product channels; reaction probabilities versus impact parameter; reaction cross sections versus reagent relative translational energy; product energy partitioning; velocity scattering angles; and reaction rate constants. Comparisons are also made with the reaction dynamics for the isoelectronic F<sup>−</sup> + CH<sub>3</sub>I reaction<sup>18</sup> and experiments for the OH<sup>−</sup> + CH<sub>3</sub>I reaction.<sup>19,31</sup>

## II. COMPUTATIONAL PROCEDURE

**A. Electronic Structure Calculations.** The NWChem computer program<sup>32,33</sup> was used to perform a range of different electronic structure calculations. MP2<sup>34</sup> and DFT,<sup>35</sup> the latter with the B97-1,<sup>36</sup> B3LYP,<sup>37</sup> and B2PLYP<sup>38</sup> functionals, were employed to investigate the ability of different electronic structure theory methods to give accurate heats of reaction for OH<sup>−</sup> + CH<sub>3</sub>I to form the CH<sub>3</sub>OH + I<sup>−</sup> and CH<sub>2</sub> + I<sup>−</sup> + H<sub>2</sub>O products, and to identify a practical and accurate level of electronic structure theory for the direct dynamics simulations. Two basis sets aug-cc-pVTZ-pp<sup>39</sup> and ECP/d<sup>29</sup> were used for both MP2 and DFT calculations. For the ECP/d basis set, Dunning and Woon’s aug-cc-pVDZ basis set<sup>40,41</sup> is used for the H, C, and O atoms. For iodine, the Wadt and Hay effective core potential (ECP)<sup>42</sup> was used for the core electrons and a 3s, 3p basis set for the valence electrons, which was augmented by a d-polarization function with a 0.262 exponent, and s, p, and d diffuse functions with exponents of 0.034, 0.039, and 0.0873, respectively. The aug-cc-pVTZ-pp basis set consists of the Peterson aug-cc-pVDZ basis set with a pseudopotential (pp) for iodine.<sup>39</sup> Experimental data<sup>43–47</sup> were used to compare heats of reaction given by above methods with experiment. From these comparisons, the B97-1/ECP/d method was chosen for the direct dynamics simulations. This is the same method used for the direct dynamics simulations of the isoelectronic F<sup>−</sup> + CH<sub>3</sub>I reaction.<sup>18</sup>

To characterize the OH<sup>−</sup> + CH<sub>3</sub>I PES, the B97-1/ECP/d method was used to search for stationary points and determine their structures, vibrational frequencies, and energies.

**B. Direct Dynamics Simulations.** As described above, the direct dynamics simulations<sup>48</sup> for the OH<sup>−</sup> + CH<sub>3</sub>I reaction were performed with the B97-1/ECP/d level of theory. The trajectories for the simulations were calculated with the VENUS chemical dynamics computer program<sup>49,50</sup> interfaced with the NWChem electronic structure computer program.<sup>32,33</sup> To directly compare with the experiments of the Wester research group, initial conditions for the trajectories were selected for collision energies (i.e., reagent relative translational energy)  $E_{\text{rel}}$  of 0.05, 0.5, 1.0, and 2.0 eV, and CH<sub>3</sub>I vibrational and rotational temperatures of  $T_v = 330$  K and  $T_r = 130$  K. The experimental vibrational and rotational temperatures for OH<sup>−</sup> are 100 K. OH<sup>−</sup> was prepared in the  $n = 0$  ground vibrational state, because this is the only state appreciably populated at 100 K. To have a rotational energy representative of the experimental distribution of energies, OH<sup>−</sup> was prepared in the  $J = 3$  rotational state. Semiclassical quantization of the action integral,<sup>51</sup> for the potential  $[V(r) + J(J + 1)\hbar^2/(2\mu r^2)]$ , was performed to select initial conditions for the OH<sup>−</sup> energy level with  $n = 0$  and  $J = 3$ . Algorithms for sampling the OH<sup>−</sup> + CH<sub>3</sub>I initial conditions are standard options in VENUS and have been described previously.<sup>52</sup>

After testing different integration algorithms, we selected a sixth-order symplectic algorithm<sup>53,54</sup> with a 2.5 fs time step to integrate the trajectories. The total integration time depended on the collision energy, i.e., 1.5 ps for 0.05 and 0.5 eV, and 0.5 ps for 1.0 and 2.0 eV. Reactive trajectories were identified by viewing animations and, thus, determining their atomic-level mechanisms.

The properties determined from the simulations are the: reaction pathways and their atomic-level mechanisms; reaction cross sections for the different pathways and their individual atomistic mechanisms; distributions of the partitioning of the available energy to product vibration, rotation, and relative translation; and velocity scattering angle distributions. The above properties compared with experiment are the relative product ion yield, and the product energy and velocity scattering distributions. With the version of VENUS/NWChem used for the simulations, it is not possible to calculate the individual potential energies for two or more molecular products for a specific pathway. Thus, to calculate product vibrational energies for the CH<sub>2</sub>I<sup>−</sup> + H<sub>2</sub>O product pathway, the average potential energy of the molecular product was assumed to equal its average vibrational kinetic energy which may be calculated.

This model is exact for an ensemble of harmonic oscillators<sup>55</sup> and found to be a good approximation for the anharmonic C<sub>2</sub>H<sub>5</sub> → H + C<sub>2</sub>H<sub>4</sub> reaction dynamics.<sup>56</sup> This approach for calculating the product vibrational energy was tested by comparing the average total product energy calculated in this manner with the actual value for the simulations, which is the average reactant energy plus the classical  $\Delta E_{\text{rxn}}$ . For  $E_{\text{rel}} = 2.0$  eV the two energies agree within 0.1% and only disagree by 4, 3, and 8% for  $E_{\text{rel}}$  of 1.0, 0.5, and 0.05 eV, respectively, with the energy higher for the approximate calculation. Setting the product vibrational energy to twice the product vibrational kinetic energy is seen to be a good approximation for calculating the CH<sub>2</sub>I<sup>−</sup> and H<sub>2</sub>O vibrational energies.

### III. PROPERTIES OF THE POTENTIAL ENERGY SURFACE

**A. Comparison of Different Electronic Structure Theories.** To assess the accuracy of different electronic structure methods for the direct dynamics simulations, reaction enthalpies for the  $\text{OH}^- + \text{CH}_3\text{I}$  reaction to form the  $\text{CH}_3\text{OH} + \text{I}^-$  and  $\text{CH}_2 + \text{I}^- + \text{H}_2\text{O}$  products were calculated with the MP2, B97-1, B3LYP, and B2PLYP methods, and two basis sets, called ECP/d and aug-cc-pVTZ-pp, which are described above. Experimental thermal data at 0 K was used as a benchmark for testing and comparing these methods. The results are given in Table 1, where it is seen that the DFT methods give more

**Table 1. Comparison of Reaction Energies for Two  $\text{OH}^- + \text{CH}_3\text{I}$  Product Channels Using Different Electronic Structure Methods**

	product channels <sup>a</sup>	
	$\text{CH}_3\text{OH} + \text{I}^-$	$\text{CH}_2 + \text{I}^- + \text{H}_2\text{O}$
MP2	-58.36 (-56.52) <sup>b</sup>	34.93 (40.84)
B97-1	-64.87 (-63.56)	28.14 (30.15)
B3LYP	-64.48 (-62.92)	26.35 (28.53)
B2PLYP	-62.10 (-59.46)	29.06 (31.88)
exp	-66.44 <sup>c</sup>	26.32 <sup>c</sup>

<sup>a</sup>Calculated energies in kcal/mol include harmonic zero-point energy (ZPE) corrections. The experimental value is the 0 K heat of reaction. <sup>b</sup>The ECP/d basis set value is given in normal text, the aug-cc-pVTZ-pp value is in parentheses. <sup>c</sup>Experimental values from ref 43.

accurate energies than MP2 and the ECP/d basis is more accurate than aug-cc-pVTZ-pp. In particular B97-1 and B3LYP, with ECP/d, give energies in quite good agreement with experiment, with B3LYP performing somewhat better than B97-1. The B97-1/ECP/d method was used in the previous direct dynamics study for the  $\text{F}^- + \text{CH}_3\text{I}$  reaction<sup>18</sup> and, to facilitate comparisons with this earlier work, the B97-1 method was also used for the direct dynamics simulations reported here.

**B. Stationary Point Structures and Energies for Different Reaction Paths.** The B97-1/ECP/d method was used to calculate reaction enthalpies for different possible product channels for the  $\text{OH}^- + \text{CH}_3\text{I}$  reaction. Restricted DFT was used for these calculations, except for the open-shell products  $\text{CH}_3 + \text{IOH}^-$  for which unrestricted DFT<sup>35</sup> was used. The results are given in Table 2, where they are also compared with experimental reaction energies. The agreement between the experimental and DFT energies is quite good for all the pathways for which experimental energies are available. Experimental energies may only be approximated for the  $\text{CH}_3^- + \text{IOH}$  channel. As discussed below, the five product channels observed in the simulations are  $\text{CH}_3\text{OH} + \text{I}^-$ ,  $[\text{CH}_3\text{--I--OH}]^-$ ,  $\text{CH}_2\text{I}^- + \text{H}_2\text{O}$ ,  $\text{CH}_3 + \text{IOH}^-$ , and  $\text{CH}_2 + \text{I}^- + \text{H}_2\text{O}$ . Though the remaining three channels are energetically accessible, they were not observed in the simulations.

Energies and structures were investigated in detail for the  $\text{OH}^- + \text{CH}_3\text{I} \rightarrow \text{CH}_3\text{OH} + \text{I}^-$   $\text{S}_{\text{N}}2$  pathway using the B97-1/ECP/d method, and the results are summarized in Figure 1. As found for the  $\text{F}^- + \text{CH}_3\text{I}$  reaction,<sup>18</sup> there is a hydrogen-bonded  $\text{HO}^- \cdots \text{HCH}_2\text{I}$  prereaction complex potential minimum and a  $[\text{HO}^- \cdots \text{HCH}_2\text{--I}]^-$  transition state (TS) with hydrogen-bonding characteristics. This TS is connected to the postreaction complex  $\text{CH}_3\text{OH} \cdots \text{I}^-$ , which is also hydrogen-bonded and has

**Table 2. Reaction Enthalpies for Different  $\text{OH}^- + \text{CH}_3\text{I}$  Product Channels<sup>a</sup>**

products	$\Delta H_{\text{rxn}}$		
	0 K <sup>b</sup>	298 K <sup>b</sup>	B97-1 <sup>c</sup>
$\text{CH}_3\text{OH} + \text{I}^-$	-66.44	$-66.91 \pm 0.26$	-64.87
$[\text{CH}_3\text{--I--OH}]^-$			-26.1
$\text{IO}^- + \text{CH}_4$			-13.6
$\text{CH}_2\text{I}^- + \text{H}_2\text{O}$		$-3.12 \pm 1.82^d$	-4.23
$\text{CH}_3 + \text{IOH}^-$			11.10 <sup>e</sup>
$^1\text{CH}_2 + \text{I}^-(\text{H}_2\text{O})$	$16.04 \pm 0.72^f$	$16.49 \pm 1.89^f$	18.18
$^1\text{CH}_2 + \text{I}^- + \text{H}_2\text{O}$	26.32	$26.77 \pm 1.17$	28.14
$\text{CH}_3^- + \text{IOH}$	$43.61 \pm 0.70^g$	$46.83 \pm 2.30^g$	46.98

<sup>a</sup>Energies are in kcal/mol. <sup>b</sup>Experimental energies from refs 43 and 44. <sup>c</sup>0 K energies including harmonic zero-point energies. <sup>d</sup>For  $\text{CH}_2\text{I}^-$  the experimental enthalpy was calculated from the enthalpy of formation  $\Delta H_f^0$  of  $\text{CH}_2\text{I}^{\cdot}$  and its electron affinity.<sup>45</sup> <sup>e</sup>The unrestricted B97-1 method<sup>36</sup> is used to calculate the energy for the  $\text{CH}_3 + \text{IOH}^-$  products. <sup>f</sup>The enthalpy of  $\text{I}^-(\text{H}_2\text{O})$  is derived from the sum of the heats of formation  $\Delta H_f^0$  for  $\text{I}^-$  and  $\text{H}_2\text{O}$ ,<sup>43</sup> and the binding energy from ref 46. <sup>g</sup>The enthalpy of  $\text{CH}_3^-$  were calculated from the enthalpy of formation  $\Delta H_f^0$  for  $\text{CH}_3^{\cdot}$  and its electron affinity.<sup>47</sup>

a structure similar to that of the  $\text{CH}_3\text{OH} \cdots \text{F}^-$  complex for the  $\text{OH}^- + \text{CH}_3\text{F} \rightarrow \text{CH}_3\text{OH} + \text{F}^-$   $\text{S}_{\text{N}}2$  reaction.<sup>30</sup>

The traditional potential energy surface for a  $\text{S}_{\text{N}}2$  reaction has potential minima for the  $\text{X}^- \cdots \text{CH}_3\text{Y}$  and  $\text{XCH}_3 \cdots \text{Y}^-$  pre- and postreaction ion-dipole complexes and a  $[\text{X}^- \cdots \text{CH}_3 \cdots \text{Y}]^-$  central barrier, each with  $\text{C}_{3v}$  symmetry. This work, along with previous work,<sup>6,18,30</sup> provides evidence for nontraditional pre- and postreaction complexes, with hydrogen-bonding. The results of the dynamics simulations, presented below, show that the hydrogen-bonded prereaction complex plays an important part in indirect mechanisms for  $\text{OH}^- + \text{CH}_3\text{I}$  reaction pathways.

**C.  $[\text{CH}_3\text{--I--OH}]^-$  Intermediate.** For the  $\text{OH}^- + \text{CH}_3\text{I}$  direct dynamics simulations, the  $[\text{CH}_3\text{--I--OH}]^-$  anion intermediate was formed in some of the trajectories. A similar complex with the structure  $[\text{CF}_3\text{--X--F}]^-$  ( $\text{X} = \text{Br}, \text{I}$ ), containing a hypervalent halogen atom X, was suggested as an intermediate in the association reactions of  $\text{F}^-$  with  $\text{CH}_3\text{Br}$  and  $\text{CH}_3\text{I}$ .<sup>57</sup> Another similar complex  $[\text{CH}_3\text{--Br--Cl}]^-$  was assumed to be the intermediate to form the dihalide ionic product  $\text{ClBr}^-$  from the reaction of  $\text{Cl}^-$  with  $\text{CH}_3\text{Br}$ , an assumption supported by MP2/LANL1DZ ab initio calculation.<sup>58</sup>

In the trajectories, the  $[\text{CH}_3\text{--I--OH}]^-$  anion intermediate dissociated to either the  $\text{S}_{\text{N}}2$  products  $\text{CH}_3\text{OH} + \text{I}^-$  or proton-transfer products  $\text{CH}_2\text{I}^- + \text{H}_2\text{O}$ . For the lower collision energies of 0.5 and 0.05 eV, some of these intermediates remained intact when the trajectories were terminated, with a larger fraction remaining at the lower energy of 0.05 eV. These intermediates have sufficient energy to dissociate to  $\text{CH}_3\text{OH} + \text{I}^-$  or  $\text{CH}_2\text{I}^- + \text{H}_2\text{O}$ , and this would occur if the trajectories were run for a longer period of time.

The geometry of  $[\text{CH}_3\text{--I--OH}]^-$  was calculated with B97-1/ECP/d theory and is depicted in Figure 1. The C--I--O entity is linear and the I--O--H angle is  $103.0^\circ$ . It is of interest to compare the C--I and I--O bond lengths with those for other species, also calculated with B97-1/ECP/d. The C--I bond in  $[\text{CH}_3\text{--I--OH}]^-$  is 2.285 and 0.135 Å longer than the C--I bond in  $\text{CH}_3\text{I}$ . The I--O bond length is 2.383 Å and longer than the I--O bond of 2.003 Å for the IOH radical, but shorter than the

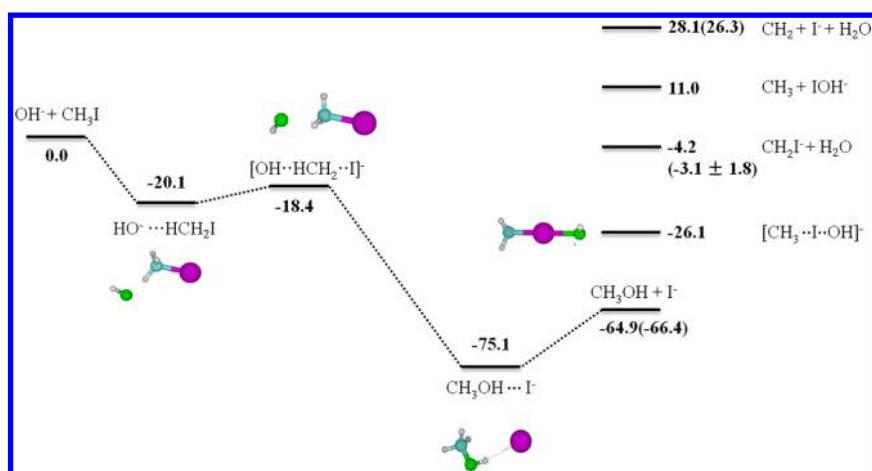


**Figure 1.** Schematic energy profile for the  $\text{OH}^- + \text{CH}_3\text{I} \rightarrow \text{CH}_3\text{OH} + \text{I}^-$  reaction at the DFT/B97-1/ECP/d level of theory, and other possible reaction channels. The energies shown are in kcal/mol and are relative to the  $\text{OH}^- + \text{CH}_3\text{I}$  reactants. Zero point energies are included. Experimental 0 K heats of reaction are in parentheses.

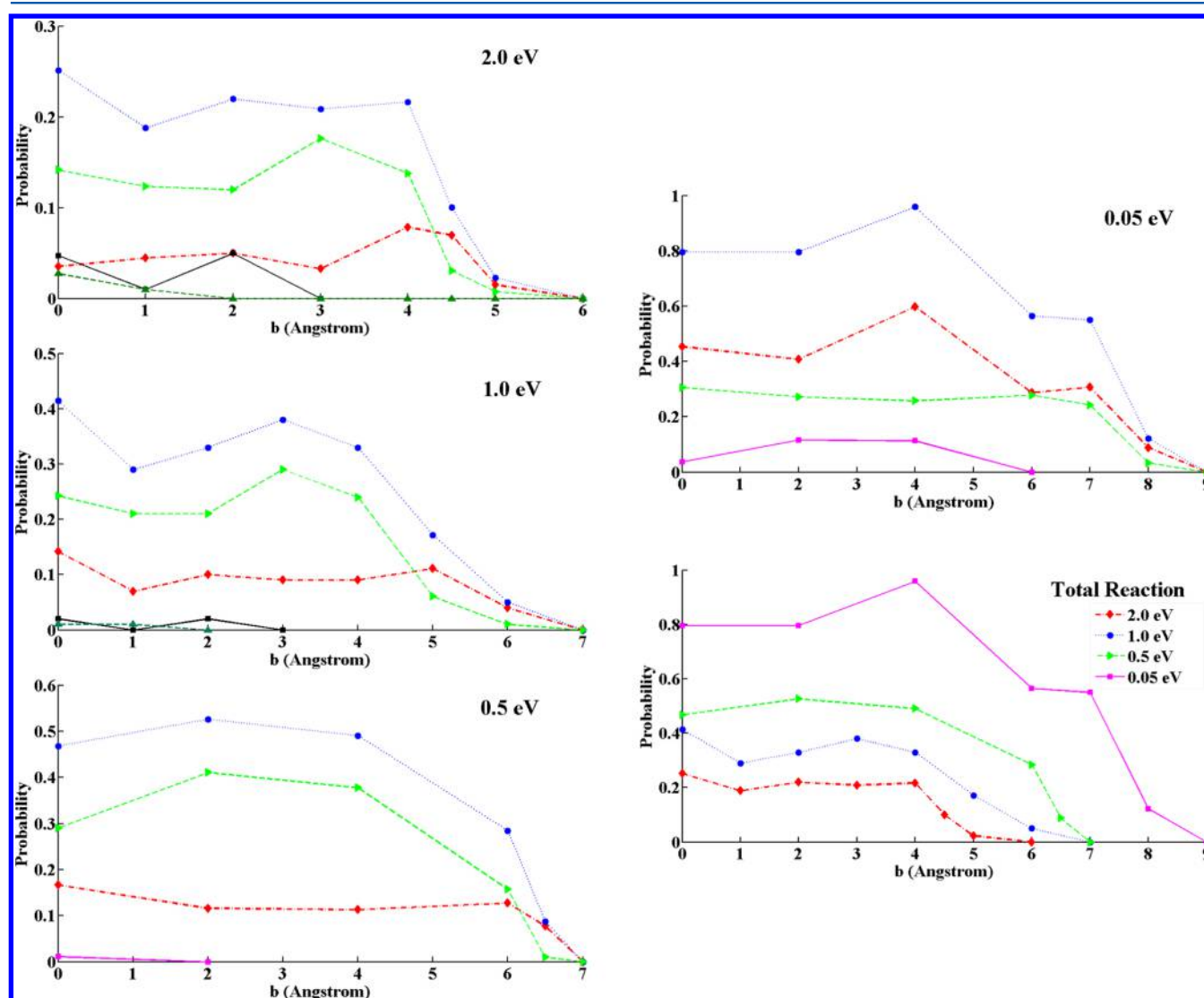


**Figure 2.** Simulation probabilities of the five  $\text{OH}^- + \text{CH}_3\text{I}$  reaction pathways versus impact parameter at  $E_{\text{rel}}$  of 2.0, 1.0, 0.5, and 0.05 eV: blue, total reaction; red,  $\text{CH}_3\text{OH} + \text{I}^-$ ; lime green,  $\text{CH}_2\text{I} + \text{H}_2\text{O}$ ; green,  $\text{CH}_2 + \text{I}^- + \text{H}_2\text{O}$ ; black,  $\text{IOH}^- + \text{CH}_3$ ; pink,  $[\text{CH}_3\text{---I---OH}]^-$ . Comparison of the total reaction probabilities for the different  $E_{\text{rel}}$  is given in the last graph.

I–O bond of 2.652 Å for the IOH<sup>−</sup> anion. The O–H bond length of [CH<sub>3</sub>--I--OH]<sup>−</sup> is 0.966 Å and significantly shorter than that for the OH radical (0.984 Å), but nearly the same as those for the OH<sup>−</sup> anion (0.969 Å), IOH radical (0.968 Å), IOH<sup>−</sup> anion (0.969), and of CH<sub>3</sub>OH (0.963 Å).

The harmonic vibrational frequencies for the intermediate are 32, 147, 150, 291, 392, 652, 738, 755, 1137, 1421, 1422, 3002, 3101, 3104, and 3820 cm<sup>−1</sup>. The largest frequency is the OH stretch, and the next six highest are the stretches and bends for the CH<sub>3</sub> moiety.

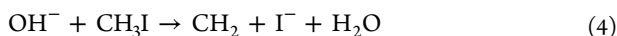
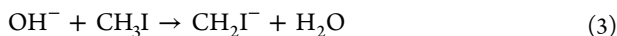
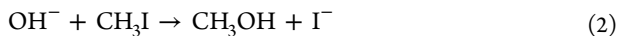
A Mulliken population analysis<sup>59,60</sup> of [CH<sub>3</sub>--I--OH]<sup>−</sup> shows the iodine atom carries a +0.5 charge. The remaining negative 1.5 charge is nearly evenly distributed between CH<sub>3</sub> and OH, with −0.72 and −0.79 charges, respectively. The charge on the carbon atom is −0.27, is −0.45 for the oxygen atom, −0.15 for the H-atoms of CH<sub>3</sub>, and −0.34 for the hydroxyl hydrogen.

As shown in Figure 1, the [CH<sub>3</sub>--I--OH]<sup>−</sup> intermediate is 26.1 kcal/mol lower in energy as compared to the reactants. Dissociation of the intermediate to the S<sub>N</sub>2 products CH<sub>3</sub>OH + I<sup>−</sup> is 38.8 kcal/mol exothermic, whereas its dissociation to the proton-transfer products CH<sub>2</sub>I<sup>−</sup> + H<sub>2</sub>O is 21.84 kcal/mol endothermic.

#### IV. COMPUTATIONAL REACTION DYNAMICS AND COMPARISON WITH EXPERIMENT

The OH<sup>−</sup> + CH<sub>3</sub>I reaction dynamics were studied at reactant relative collision energies  $E_{\text{rel}}$  of 0.05, 0.5, 1.0, and 2.0 eV, and CH<sub>3</sub>I vibrational and rotational temperatures of  $T_v = 330$  K and  $T_r = 130$  K, respectively. These conditions were chosen to match the experiments of the Wester research group. The simulations were performed versus collision impact parameter and then properly averaged to compare with experiment. For the four  $E_{\text{rel}}$ , in increasing order, a total 755, 682, 798, and 1501 trajectories were calculated.

**A. Reaction Probabilities versus Impact Parameter for Different  $E_{\text{rel}}$ .** The trajectories were calculated versus fixed impact parameter  $b$ :  $b$  of 0, 2, 4, 6, 7, 8, and 9 Å for  $E_{\text{rel}}$  of 0.05 eV; 0, 2, 4, 6, 6.5, and 7 Å for  $E_{\text{rel}}$  of 0.5 eV; 0, 1, 2, 3, 4, 5, 6, and 7 Å, for  $E_{\text{rel}}$  of 1.0 eV; 0, 1, 2, 3, 4, 4.5, 5, and 6 Å for  $E_{\text{rel}}$  of 2.0 eV. There were no reactions out of 100 trajectories at the largest  $b$  considered for each  $E_{\text{rel}}$ . The following five reaction pathways



were observed in the simulations and their reaction probabilities, and the total reaction probability are plotted in Figure 2 for each  $E_{\text{rel}}$ , versus impact parameter  $b$ , i.e.,  $P_r(b)$ . The energies for these pathways are compared in Figure 1 and Table 2. The results in Figure 2 show that the reaction probability decreases with increase in  $E_{\text{rel}}$ . This trend is reasonable given the long-range attraction between the reactants. As  $E_{\text{rel}}$  is increased, this attraction is less efficient at pulling the reactants together and the reaction probability decreases. With lower  $E_{\text{rel}}$  there is also a longer interaction time between the reactants, which will assist in attaining their proper alignment for reaction.

Reaction 2 is the S<sub>N</sub>2 reaction, but it only dominates at the smallest  $E_{\text{rel}}$  of 0.05 eV. For the higher  $E_{\text{rel}}$  of 0.5, 1.0, and 2.0 eV it has a smaller percentage than does the competing reaction 3. Reactions 2 and 3 together comprise more than 93% of all reactive trajectories for each  $E_{\text{rel}}$ . Reaction 4 was observed for collision energies of 2.0 and 1.0 eV. The IOH<sup>−</sup> anion was only formed at 2.0 eV, where it comprised only ~2% of the product ions. The [CH<sub>3</sub>--I--OH]<sup>−</sup> complex in reaction 6 was only observed at the conclusion of the trajectories for  $E_{\text{rel}}$  of 1.0 eV and lower. It is an intermediate which has sufficient energy to dissociate if the trajectories were run for a longer period of time. Here we also include it as a reaction pathway.

**B. Atomic-Level Mechanisms.** Reactions 2 and 3 are the most important pathways, and there is an interest in determining their atomic-level mechanisms. This was done by animating each trajectory for these reactions and identifying if the reaction was direct or indirect. Example animations of the trajectories are on the Web site monte.chem.ttu.edu.

Reaction 2 has both direct and indirect mechanisms, with three different direct mechanisms called direct rebound, direct stripping, and front side attack. For the rebound mechanism, OH<sup>−</sup> attacks the backside of CH<sub>3</sub>I, directly replaces I<sup>−</sup>, and reverses its direction with CH<sub>3</sub> attached. Stripping occurs when OH<sup>−</sup> approaches CH<sub>3</sub>I on its side and directly strips away the CH<sub>3</sub> group. These two mechanisms were observed in previous simulations of the F<sup>−</sup> + CH<sub>3</sub>I<sup>18</sup> and Cl<sup>−</sup> + CH<sub>3</sub>Y (Y = Cl,<sup>26</sup> Br,<sup>28</sup> I<sup>17</sup>) S<sub>N</sub>2 reactions. As shown in Table 3, the direct rebound mechanism occurs for small impact parameters, whereas the stripping mechanism is a larger impact parameter event. For front side attack, OH<sup>−</sup> attacks the C–I bond from the side and directly substitutes I<sup>−</sup>. The stereochemistry of CH<sub>3</sub> is preserved for this mechanism.

For the HO<sup>−</sup> + CH<sub>3</sub>I S<sub>N</sub>2 reaction there are several different indirect mechanisms, including roundabout, formation of the HO<sup>−</sup>---HCH<sub>2</sub>I hydrogen-bonded prereaction complex, central barrier recrossing, proton exchange, and couplings of these events. For the roundabout mechanism, OH<sup>−</sup> strikes the side of CH<sub>3</sub>, causing CH<sub>3</sub> to rotate around the massive I atom one or two times. Then OH<sup>−</sup> attacks the back side of the C atom and directly substitutes I<sup>−</sup>. This mechanism was first reported for the Cl<sup>−</sup> + CH<sub>3</sub>I → ClCH<sub>3</sub> + I<sup>−</sup> reaction<sup>17</sup> and was also observed for the F<sup>−</sup> + CH<sub>3</sub>I reaction.<sup>18</sup> For two of the trajectories reaction occurred by the roundabout mechanism, but with retention of the CH<sub>3</sub> stereochemistry, a quite interesting finding. As CH<sub>3</sub> rotates about the massive I atom, instead of attacking the back side of the C atom, OH<sup>−</sup> attacks the front side of C atom, without inversion of the CH<sub>3</sub>-group to form the CH<sub>3</sub>OH product.

As discussed below, except at  $E_{\text{rel}}$  of 2.0 eV, the dominant indirect mechanism involves formation of hydrogen-bonded complex HO<sup>−</sup>---HCH<sub>2</sub>I, for which HO<sup>−</sup> interacts attractively with one or more of the H atoms and the system becomes temporarily trapped in the prereaction potential energy well. Then, HO<sup>−</sup> attacks the C atom backside and displaces I<sup>−</sup>. The lifetime of the HO<sup>−</sup>---HCH<sub>2</sub>I complex ranges from 125 to 650 fs, which is quite short compared to the F<sup>−</sup>---HCH<sub>2</sub>I complex lifetime of 150 fs to 3 ps for the F<sup>−</sup> + CH<sub>3</sub>I reaction.<sup>18</sup> Barrier recrossing was observed previously in the dynamics for Cl<sup>−</sup> + CH<sub>3</sub>Cl,<sup>22,27</sup> Cl<sup>−</sup> + CD<sub>3</sub>Cl,<sup>6</sup> and Cl<sup>−</sup> + CH<sub>3</sub>I.<sup>17</sup>

For the proton exchange mechanism, OH<sup>−</sup> attracts a H atom from CH<sub>3</sub> to become a H<sub>2</sub>O molecule and forming CH<sub>2</sub>I<sup>−</sup>. In some trajectories, the H<sub>2</sub>O molecule does not have sufficient translational energy to overcome the CH<sub>2</sub>I<sup>−</sup> attraction, so it first

**Table 3. Percentages of Different Atomic-Level Mechanisms versus Impact Parameter for the  $\text{OH}^- + \text{CH}_3\text{I} \rightarrow \text{CH}_3\text{OH} + \text{I}^-$   $\text{S}_{\text{N}}2$  Reaction**

$b^a$	direct <sup>c</sup>		indirect
	DR	DS	
$E_{\text{rel}} = 2.0 \text{ eV}$			
0	56	0	44
1	56	0	44
2 <sup>b</sup>	80	0	0
3	100	0	0
4	0	100	0
4.5	0	100	0
5	0	100	0
$E_{\text{rel}} = 1.0 \text{ eV}$			
0	64	0	36
1	43	0	57
2	70	10	20
3	44	33	23
4	0	78	22
5	0	82	18
6	0	100	0
$E_{\text{rel}} = 0.5 \text{ eV}$			
0	61	0	39
2	45	0	55
4	33	42	25
6	0	38	62
6.5	0	87	13
$E_{\text{rel}} = 0.05 \text{ eV}$			
0	53	0	47
2	64	0	36
4	59	12	29
6	0	69	31
7	0	46	54
8	0	62	38

<sup>a</sup>The impact parameter  $b$  is in units of Å. <sup>b</sup>20% of the direct mechanisms is front side attack. <sup>c</sup>DR and DS are direct rebound and direct stripping, respectively.

remains attracted to  $\text{CH}_2\text{I}^-$  forming a  $\text{CH}_2\text{I}^- \cdots \text{H}_2\text{O}$  complex. There are two types of intermolecular motions for this complex: for one  $\text{H}_2\text{O}$  vibrates extensively with respect to  $\text{CH}_2\text{I}^-$ , and for the other  $\text{H}_2\text{O}$  rotates about its center of mass and/or around the I atom. Ultimately,  $\text{H}_2\text{O}$  gives back a H atom to  $\text{CH}_2\text{I}^-$  forming the  $\text{OH}^- \cdots \text{HCH}_2\text{I}$  complex, followed by  $\text{OH}^-$  attack of the C atom backside, displacing  $\text{I}^-$ . The lost and gain of a proton by  $\text{OH}^-$  occurs one or several times between the same or different H's. This proton exchange mechanism for forming  $\text{CH}_3\text{OH} + \text{I}^-$  is always coupled with the prereaction complex mechanism.

For a small number of the trajectories the structure of the  $[\text{CH}_3\text{-I-OH}]^-$  intermediate participates in the  $\text{S}_{\text{N}}2$  and proton-transfer pathways by coupling with the roundabout mechanism. For this mechanism  $\text{OH}^-$  initially strikes either the I-atom or the side of the  $\text{CH}_3$ -group, resulting in  $\text{CH}_3$  rotation about the massive I-atom. If  $\text{OH}^-$  strikes the I-atom first, there are events in which a transient  $[\text{CH}_3\text{-I-OH}]^-$  intermediate is formed before  $\text{CH}_3$  begins its rotation about the I-atom. After one or two  $\text{CH}_3$  rotations,  $\text{OH}^-$  reacts with  $\text{CH}_3\text{I}$  producing either  $\text{CH}_3\text{OH} + \text{I}^-$  or  $\text{CH}_2\text{I}^- + \text{H}_2\text{O}$ .

An important finding from the trajectories is that although the hydrogen-bonded postreaction complex  $\text{CH}_3\text{OH} \cdots \text{I}^-$  is a potential minimum on the  $\text{S}_{\text{N}}2$  reaction pathway, this complex was not formed in any of the 3736 trajectories calculated here for  $E_{\text{rel}}$  of 0.05–2.0 eV. The trajectories either pass through<sup>20</sup> or pass by<sup>30</sup> this minimum without forming a complex.

**C. Reaction Cross Sections versus  $E_{\text{rel}}$ .** The total reaction cross section  $\sigma_r$  was obtained by integrating the total reaction probability  $P_r(b)$  over the impact parameter according to  $\int P_r(b) 2\pi b db$ . The resulting cross section increases with decrease in the collision energy and is  $4.3 \pm 1.0$ ,  $10.9 \pm 3.1$ ,  $16.5 \pm 4.3$ , and  $75.5 \pm 9.6 \text{ \AA}^2$  for  $E_{\text{rel}}$  of 2.0, 1.0, 0.5, and 0.05 eV, respectively. The individual cross sections for the five reaction pathways, observed in simulations, are listed in Table 4.

**1.  $\text{CH}_3\text{OH} + \text{I}^-$  Product Pathway.** Cross sections were calculated for the different atomic-level mechanisms for the  $\text{S}_{\text{N}}2$  pathway forming the  $\text{CH}_3\text{OH} + \text{I}^-$  products. The respective cross sections for the direct rebound, direct stripping, and indirect mechanisms are  $1.3 \pm 0.6$ ,  $2.8 \pm 0.7$ , and  $0.2 \pm 0.1$ ;  $2.0 \pm 0.9$ ,  $6.8 \pm 2.2$ , and  $2.1 \pm 1.5$ ;  $3.9 \pm 1.9$ ,  $5.8 \pm 2.1$ , and  $6.9 \pm 2.3$ ; and  $25.2 \pm 3.6$ ,  $21.3 \pm 4.3$ , and  $29.5 \pm 5.2 \text{ \AA}^2$  for  $E_{\text{rel}}$  of 2.0, 1.0, 0.5, and 0.05 eV, respectively. Fractions of the different reaction mechanisms are summarized in Figure 3 for the four collision energies from 0.05 to 2.0 eV. Included are the individual indirect mechanisms: i.e.,  $\text{HO}^- \cdots \text{HCH}_2\text{I}$  prereaction complex (A); roundabout mechanism (Ra); barrier recrossing (br); proton exchange (PE); proton exchange with  $\text{H}_2\text{O}$  rotation (PER); and couplings between these mechanisms. For each  $E_{\text{rel}}$  the direct mechanisms dominate with a fraction of 0.58 to 0.97, with direct stripping most important except for the lowest  $E_{\text{rel}}$ . Overall, the fraction of the indirect mechanism increases with lower  $E_{\text{rel}}$ , i.e., 3%, 19%, 42%, and 39% at  $E_{\text{rel}}$  of 2.0, 1.0, 0.5, and 0.05 eV, respectively.

A feature that emerges with smaller  $E_{\text{rel}}$  is the increase in the types of indirect mechanisms. At  $E_{\text{rel}}$  of 2.0 eV, only the roundabout mechanism occurs. Three more indirect mechanisms, i.e., unmixed hydrogen-bonded complex  $\text{HO}^- \cdots \text{HCH}_2\text{I}$  formation, coupling of this complex formation with barrier recrossing, and proton exchange, emerge with a decrease in  $E_{\text{rel}}$

**Table 4. Cross Sections versus  $E_{\text{rel}}$  for the Different Reaction Pathways<sup>a</sup>**

pathway	$E_{\text{rel}}$			
	2.0	1.0	0.5	0.05
$\text{CH}_3\text{OH} + \text{I}^-$	$4.3 \pm 1.0$	$10.9 \pm 3.1$	$16.5 \pm 4.3$	$76.0 \pm 9.7$
$\text{CH}_2\text{I}^- + \text{H}_2\text{O}$	$8.8 \pm 1.6$	$18.1 \pm 3.2$	$37.8 \pm 4.7$	$47.6 \pm 7.3$
$\text{CH}_2 + \text{I}^- + \text{H}_2\text{O}$	$0.8 \pm 0.5$	$0.16 \pm 0.16$	0	0
$\text{IOH}^- + \text{CH}_3$	$0.11 \pm 0.07$	0	0	0
$[\text{CH}_3\text{-I-OH}]^-$	0	$0.08 \pm 0.08$	$0.07 \pm 0.07$	$8.9 \pm 2.4$
Total	$14.0 \pm 1.9$	$29.2 \pm 4.2$	$54.3 \pm 5.4$	$132.5 \pm 10.3$

<sup>a</sup> $E_{\text{rel}}$  is in eV and the cross section is in  $\text{\AA}^2$ .

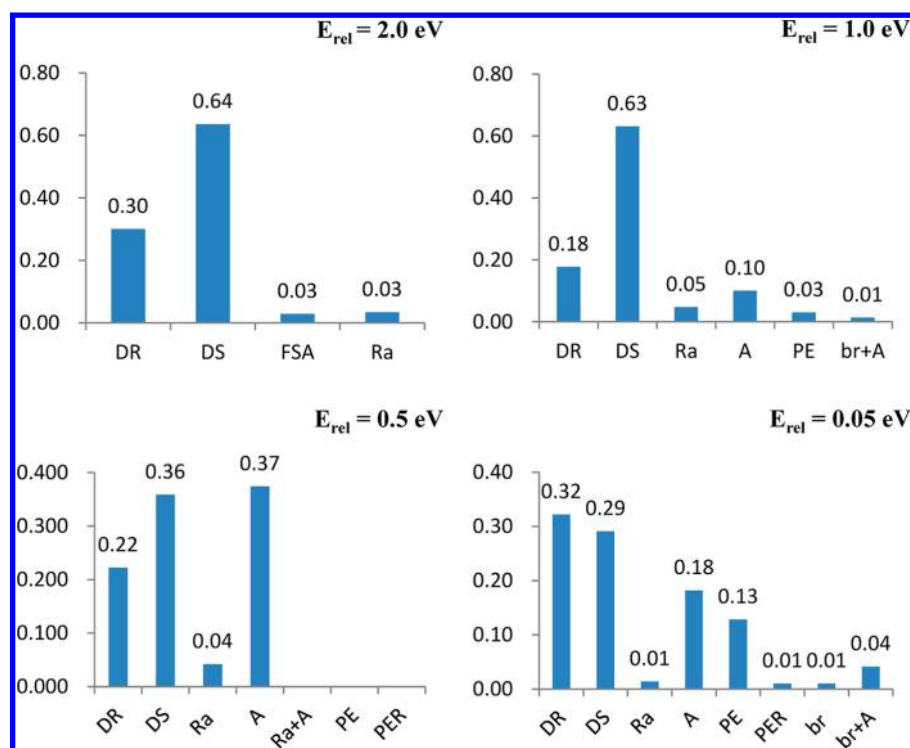


**Figure 3.** Fractions of the individual atomistic reaction mechanisms, for the  $\text{OH}^- + \text{CH}_3\text{OH} \rightarrow \text{CH}_3\text{OH} + \text{I}^-$   $\text{S}_{\text{N}}2$  reaction, at the different  $E_{\text{rel}}$ : DR, direct rebound; DS, direct stripping; Ra, roundabout; A,  $\text{HO}^- \cdots \text{HCH}_2\text{I}$ ; br, barrier recrossing; PE, proton exchange; PER, proton exchange rotation. The fractions are based on the cross sections. For  $E_{\text{rel}} = 0.5 \text{ eV}$ , the probabilities of Ra+A, PE and PER are 0.001.

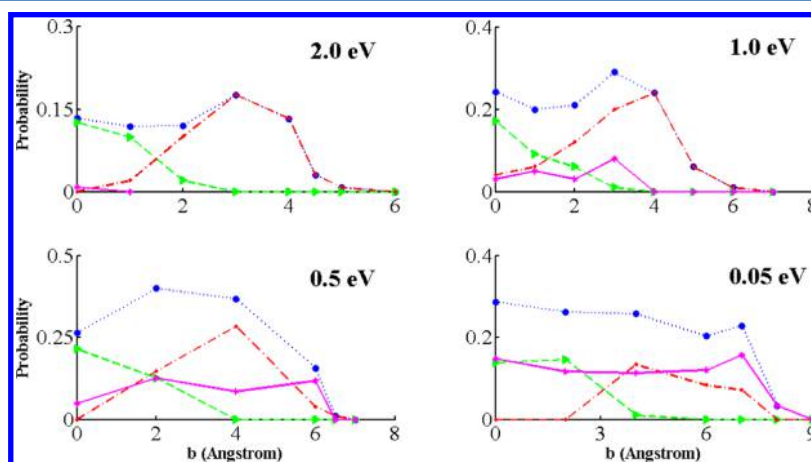


**Figure 4.** Simulation probabilities, versus impact parameter, of the three atomic-level mechanisms and total reaction for the  $\text{OH}^- + \text{CH}_3\text{I} \rightarrow \text{CH}_2\text{I}^- + \text{H}_2\text{O}$  reaction: lime green,  $\blacktriangleright$ , direct rebound; red,  $\blacklozenge$ , direct stripping; pink,  $\blacksquare$ , indirect; blue,  $\bullet$ , total reaction.

to 1.0 eV. It is notable that each of these mechanisms involve formation of the  $\text{HO}^- \cdots \text{HCH}_2\text{I}$  complex. At the lower  $E_{\text{rel}}$  of 0.5 eV, proton exchange with rotation (see above) and coupling of  $\text{HO}^- \cdots \text{HCH}_2\text{I}$  complex formation with the roundabout mechanism become contributing pathways. At the lowest  $E_{\text{rel}}$  of 0.05 eV there are six different indirect mechanisms! This multitude of indirect mechanisms illustrates the diverse and complex overall reaction mechanism for the gas phase  $\text{OH}^- + \text{CH}_3\text{I}$   $\text{S}_{\text{N}}2$  reaction.

Except at  $E_{\text{rel}}$  of 2.0 eV, where the  $\text{HO}^- \cdots \text{HCH}_2\text{I}$  complex is not formed, formation of this complex is the most important indirect pathway. Including its couplings with other mechanisms, it contributes a fraction of 0.14, 0.38, and 0.36 to the overall  $\text{S}_{\text{N}}2$  reaction at 1.0, 0.5, and 0.05 eV, respectively.

**2.  $\text{CH}_2\text{I}^- + \text{H}_2\text{O}$  Product Pathway.** Formation of the  $\text{H}_2\text{O} + \text{CH}_2\text{I}^-$  products, reaction 3, occurs at all collision energies. As for the  $\text{S}_{\text{N}}2$  pathway, this proton transfer also occurs via the direct rebound, direct stripping, and indirect mechanisms. The probabilities for these mechanisms are plotted versus impact parameter in Figure 4, where it is seen that stripping is the most important mechanism at  $E_{\text{rel}}$  of 2.0, 1.0, and 0.5 eV, and the indirect mechanisms become most important at  $E_{\text{rel}} = 0.05 \text{ eV}$ . The respective cross sections for the direct rebound, direct stripping, and indirect mechanisms are  $1.1 \pm 0.1$ ,  $7.7 \pm 1.4$ , and  $0.01 \pm 0.01$ ;  $1.8 \pm 0.5$ ,  $14.0 \pm 2.5$ , and  $2.3 \pm 0.8$ ;  $4.5 \pm 1.2$ ,  $19.7 \pm 3.1$ , and  $12.6 \pm 3.4$ ; and  $5.1 \pm 1.2$ ,  $14.2 \pm 4.3$ , and  $24.4 \pm 6.3 \text{ \AA}^2$  for  $E_{\text{rel}}$  of 2.0, 1.0, 0.5, and 0.05 eV, respectively. Direct stripping contributes 87%, 78%, and 54% of the reaction for  $E_{\text{rel}}$  of 2.0, 1.0, and 0.5 eV, respectively. The contribution of the

indirect mechanisms is negligible at 2.0 eV, i.e.,  $\sim 1\%$ , but dominant at the much lower collision energy of 0.05 eV, where they contribute 56%. The contribution of the rebound mechanism is never larger than 12%, the percentage at 2.0, 1.0, and 0.05 eV.

The two direct mechanisms for the proton-transfer reaction are quite similar to those for the  $S_N2$  reaction. There are multiple indirect mechanisms, i.e., the roundabout, formation of the  $\text{HO}^- \cdots \text{HCH}_2\text{I}$  complex, formation of the  $\text{CH}_2\text{I}^- \cdots \text{HOH}$  complex, and their combinations. The fractions of the different indirect mechanisms are displayed in Figure 5. For the

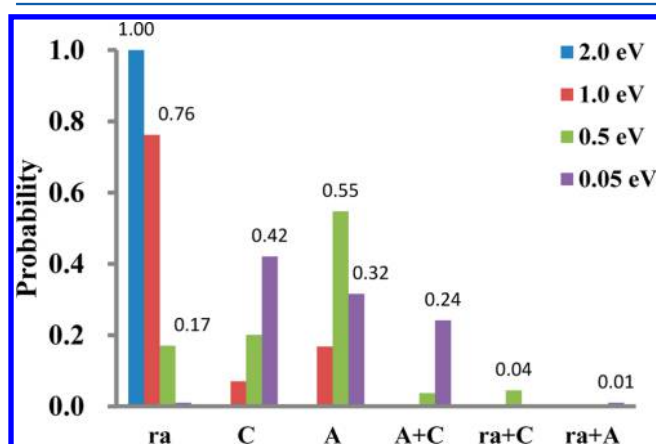


**Figure 5.** Fraction of the indirect mechanisms for the  $\text{CH}_2\text{I}^- + \text{H}_2\text{O}$  product pathway at the different  $E_{\text{rel}}$ : ra, roundabout; A,  $\text{HO}^- \cdots \text{HCH}_2\text{I}$ ; C,  $\text{CH}_2\text{I}^- \cdots \text{HOH}$ .

mechanism where both the  $\text{HO}^- \cdots \text{HCH}_2\text{I}$  and  $\text{CH}_2\text{I}^- \cdots \text{HOH}$  complexes are involved, proton exchange between the C and O atoms occurred for some of the trajectories. The roundabout mechanism is the most important indirect mechanism at  $E_{\text{rel}}$  of 2.0 and 1.0 eV, where its fractional contribution is 1.00 and 0.76, respectively. The fraction of trajectories for which the  $\text{HO}^- \cdots \text{HCH}_2\text{I}$  complex is involved is 0.17, 0.58, and 0.57 for  $E_{\text{rel}}$  of 1.0, 0.5, and 0.05 eV, respectively. The fraction of trajectories for which the  $\text{CH}_2\text{I}^- \cdots \text{HOH}$  complex is involved is 0.07, 0.28, and 0.66, for these respective  $E_{\text{rel}}$ .

**3. Comparison with Experiment.** Three of the product anions formed in the trajectories, i.e.,  $\text{I}^-$ ,  $\text{CH}_2\text{I}^-$ , and  $\text{IOH}^-$ , were detected in the experiments. The fourth species observed at the end of the simulations,  $[\text{CH}_3\text{-I-OH}]^-$ , is an intermediate and would dissociate if the trajectories were calculated for a longer time. It is not observed experimentally. As shown in Table 5, if statistical uncertainties are considered, the experiments and simulations give similar product anion

ratios at  $E_{\text{rel}}$  of 2.0 and 1.0 eV. Overall, the simulations form fewer  $\text{I}^-$  and more  $\text{CH}_2\text{I}^-$  ions than found in the experiments. This difference is most apparent at  $E_{\text{rel}}$  of 0.5 eV where the dominant ion experimentally is  $\text{I}^-$ , in contrast to the  $\text{CH}_2\text{I}^-$  ion for the simulations.

**D. Reaction Rate Constant.** The overall reaction rate constant for the simulation is given by  $k(E_{\text{rel}}, T_v, T_r) = \nu(E_{\text{rel}}) \sigma_r(E_{\text{rel}}, T_v, T_r)$ , where  $\nu(E_{\text{rel}})$  is the  $\text{OH}^- + \text{CH}_3\text{I}$  relative velocity,  $T_v$  is the vibrational temperature 330 K,  $T_r$  is the rotational temperature 130 K, and  $\sigma_r$  is the total reaction cross section from simulation. The resulting rate constant from the simulation is  $7.3 \pm 1.0$ ,  $11.1 \pm 1.6$ ,  $15.4 \pm 1.5$ , and  $20.3 \pm 1.6$  ( $10^{-10} \text{ cm}^3 \text{ mol}^{-1} \text{ s}^{-1}$ ) for  $E_{\text{rel}}$  at 2.0, 1.0, 0.5, and 0.05 eV, respectively. The rate constant at 0.05 eV is in good agreement with the experimental rate constant<sup>60</sup> of  $(15.8 \pm 2.1) \times 10^{-10} \text{ cm}^3 \text{ s}^{-1} \text{ mol}^{-1}$  at this collision energy.

**E. Product Energy Partitioning and Comparison with Experiment.** **1.  $\text{OH}^- + \text{CH}_3\text{I} \rightarrow \text{CH}_3\text{OH} + \text{I}^-$ .** Average fractions of energy partitioned to product relative translation, rotation, and vibration for the  $\text{OH}^- + \text{CH}_3\text{I} \rightarrow \text{CH}_3\text{OH} + \text{I}^-$  reaction are summarized in Table 6. The rotation and vibration fractions are also combined to denote the  $\text{CH}_3\text{OH}$  internal energy. The fractions are given for the direct rebound, direct stripping, and composite indirect mechanisms, and for the total reaction. The majority of the product energy is partitioned to  $\text{CH}_3\text{OH}$  internal energy, with the fraction increasing from  $0.68 \pm 0.02$  to  $0.80 \pm 0.01$  with decrease in  $E_{\text{rel}}$  from 2.0 to 0.05 eV, a result consistent with more indirect reaction with decrease in  $E_{\text{rel}}$ .

As shown in Table 6, the product energy partitioning differs for the different atomic-level mechanisms. For each  $E_{\text{rel}}$ , the indirect mechanisms partition more energy to  $\text{CH}_3\text{OH}$  internal energy than do the direct mechanisms. As described above in section IV.B, there are more interactions and energy exchange for the indirect mechanisms and this is expected to enhance partitioning to the multiple  $\text{CH}_3\text{OH}$  internal degrees of freedom. For the indirect mechanisms there is a small variation in  $f_{\text{int}}$  between 0.79 and 0.86 for the four  $E_{\text{rel}}$ 's. This partitioning to  $f_{\text{int}}$  by the indirect mechanisms is primarily to vibration, with the largest fraction to rotation of  $0.13 \pm 0.03$  at  $E_{\text{rel}} = 1.0$  eV. Within statistical uncertainties, the ratio of  $f_{\text{vib}}$  to  $f_{\text{rot}}$  is independent of  $E_{\text{rel}}$  for the indirect mechanisms.

There are interesting relationships between the energy partitioning for the direct mechanisms. The  $\text{CH}_3\text{OH}$  internal energy partitioning for the direct stripping mechanism is similar, i.e.,  $\sim 0.70$ , for the different  $E_{\text{rel}}$ , except for a somewhat higher value at  $E_{\text{rel}}$  of 1.0 eV. In contrast, for the direct rebound mechanism the internal energy fraction increases as the initial collision energy decreases, from 0.60 at 2.0 eV to 0.79 at 0.05 eV. This striking difference between the two direct mechanisms

**Table 5. Comparison of Product Anion Ratios for the  $\text{CH}_3\text{I} + \text{OH}^-$  Reaction from Experiment and Simulation<sup>a</sup>**

$E_{\text{rel}}$ (eV)		$\text{I}^-$	$\text{CH}_2\text{I}^-$	$\text{IOH}^-$	$[\text{CH}_3\text{-I-OH}]^-$
2.00	simulation	$0.36 \pm 0.09$	$0.63 \pm 0.11$	0.01	0.00
	experiment	0.46	0.52	0.02	0.00
1.00	simulation	$0.38 \pm 0.10$	$0.62 \pm 0.11$	0.00	<0.001
	experiment	0.40	0.60	0.00	0.00
0.50	simulation	$0.31 \pm 0.08$	$0.69 \pm 0.09$	0.00	<0.001
	experiment	0.56	0.44	0.00	0.00
0.05	simulation	$0.53 \pm 0.07$	$0.39 \pm 0.06$	0.00	$0.08 \pm 0.02$

<sup>a</sup>The experimental results at 2.0 eV were reported previously in ref 31. The  $[\text{CH}_3\text{-I-OH}]^-$  intermediate observed in the simulations would dissociate if the trajectories were calculated for a longer time.

**Table 6. Average Fractions of  $\text{OH}^- + \text{CH}_3\text{I} \rightarrow \text{CH}_3\text{OH} + \text{I}^-$  Product Energy Partitioning<sup>a</sup>**

	$f_{\text{rel}}'$	$f_{\text{rot}}'$	$f_{\text{vib}}'$	$f_{\text{int}}'$
$E_{\text{rel}} = 2.0 \text{ eV}$				
DR	0.40 ± 0.05	0.14 ± 0.03	0.46 ± 0.04	0.60 ± 0.05
DS	0.29 ± 0.01	0.18 ± 0.03	0.53 ± 0.03	0.71 ± 0.03
ind	0.21 ± 0.10	0.06 ± 0.05	0.73 ± 0.08	0.79 ± 0.08
total	0.32 ± 0.02	0.18 ± 0.02	0.50 ± 0.02	0.68 ± 0.02
exp				0.71 ± 0.03
$E_{\text{rel}} = 1.5 \text{ eV}$				
exp				0.67 ± 0.03
$E_{\text{rel}} = 1.0 \text{ eV}$				
DR	0.40 ± 0.04	0.09 ± 0.01	0.51 ± 0.04	0.60 ± 0.04
DS	0.23 ± 0.02	0.14 ± 0.03	0.63 ± 0.04	0.77 ± 0.04
ind	0.15 ± 0.02	0.13 ± 0.03	0.72 ± 0.03	0.85 ± 0.03
total	0.24 ± 0.02	0.13 ± 0.01	0.63 ± 0.02	0.76 ± 0.02
exp				0.71 ± 0.04
$E_{\text{rel}} = 0.5 \text{ eV}$				
DR	0.27 ± 0.03	0.19 ± 0.02	0.54 ± 0.03	0.73 ± 0.03
DS	0.31 ± 0.03	0.04 ± 0.01	0.65 ± 0.03	0.69 ± 0.03
ind	0.18 ± 0.02	0.11 ± 0.02	0.71 ± 0.03	0.82 ± 0.03
total	0.25 ± 0.02	0.09 ± 0.01	0.66 ± 0.02	0.75 ± 0.02
exp				0.66 ± 0.04
$E_{\text{rel}} = 0.05 \text{ eV}$				
DR	0.21 ± 0.01	0.16 ± 0.01	0.63 ± 0.01	0.79 ± 0.01
DS	0.27 ± 0.01	0.07 ± 0.01	0.66 ± 0.01	0.73 ± 0.01
ind	0.14 ± 0.01	0.09 ± 0.01	0.77 ± 0.01	0.86 ± 0.01
total	0.20 ± 0.01	0.10 ± 0.01	0.70 ± 0.01	0.80 ± 0.01

<sup>a</sup>The  $f$ 's are fractions of energy partitioned to product relative translational, rotational, and vibrational energy. DR, DS, and ind denote energy partitioning for the direct rebound, direct stripping, and indirect mechanisms, respectively. "Total" is the combined energy partitioning for these mechanisms. The B97-1/ECP/d harmonic ZPE was removed from the vibrational energy of the simulation results.  $f_{\text{rel}}' + f_{\text{int}}' = 1$  for both the simulations and experiments.

results in a "flipping" in the relative importance of partitioning to their internal energies. At  $E_{\text{rel}}$  of 2.0 and 1.0 eV direct stripping has a larger internal energy fraction than does direct rebound. For  $E_{\text{rel}}$  of 0.5 and 0.05 eV this is reversed with the fraction partitioned to internal energy larger for direct rebound. This flipping primarily results from the much larger  $f_{\text{rot}}'$  for the rebound mechanism at  $E_{\text{rel}}$  of 0.5 and 0.05 eV. For direct rebound  $f_{\text{vib}}'$  is the same for the  $E_{\text{rel}}$  except at 0.05 eV, where it is larger. In contrast, for direct stripping  $f_{\text{vib}}'$  is larger at  $E_{\text{rel}}$  of 2.0 eV and the same for the remaining  $E_{\text{rel}}$ .

The most extensive total partitioning of energy to  $\text{CH}_3\text{OH}$  rotation is for  $E_{\text{rel}} = 2.0 \text{ eV}$ , where  $f_{\text{rot}}'$  is 0.18. For direct stripping the largest  $f_{\text{rot}}'$  is 0.18 at  $E_{\text{rel}}$  of 2.0 eV, whereas for direct rebound the largest  $f_{\text{rot}}'$  is 0.19 at  $E_{\text{rel}}$  of 0.5 eV. The value of  $f_{\text{rot}}'$  for the indirect mechanisms is less than 0.13 for each of the  $E_{\text{rel}}$ .

The agreement between the simulation and experimental  $f_{\text{int}}'$  is quite good except for  $E_{\text{rel}}$  of 0.5 eV, where the experimental fraction is slightly lower. The simulation and experimental relative translational energy distributions for the  $\text{CH}_3\text{OH} + \text{I}^-$  products are compared in Figure 6 and it is seen that they are in overall quite good agreement.

2.  $\text{OH}^- + \text{CH}_3\text{I} \rightarrow \text{CH}_2\text{I}^- + \text{H}_2\text{O}$ . The average energy partitioning to the product rotational, vibrational, and relative translational degrees of freedom is given in Table 7 for the total  $\text{OH}^- + \text{CH}_3\text{I} \rightarrow \text{CH}_2\text{I}^- + \text{H}_2\text{O}$  reaction. The partitioning to relative translation is large at  $E_{\text{rel}} = 2.0 \text{ eV}$  with  $f_{\text{rel}}' = 0.71 \pm$

0.03 but then decreases to  $0.38 \pm 0.03$  at  $E_{\text{rel}} = 0.05 \text{ eV}$ . Except for the 2.0 eV collisions, a substantially larger fraction of energy is transferred to  $\text{CH}_2\text{I}^-$  than  $\text{H}_2\text{O}$ , which is primarily a result of the large rotational energies transferred to  $\text{CH}_2\text{I}^-$ . For  $\text{H}_2\text{O}$   $f_{\text{vib}}'$  and  $f_{\text{rot}}'$  are independent of  $E_{\text{rel}}$ . For the  $\text{CH}_2\text{I}^-$  product  $f_{\text{vib}}'$  increases with decrease in  $E_{\text{rel}}$ .

The agreement between the simulation and experimental  $f_{\text{rel}}'$  is quite good except for  $E_{\text{rel}}$  of 2.0 eV, where the experimental fraction is slightly lower. The simulation and experimental relative translational energy distributions for the  $\text{CH}_2\text{I}^- + \text{H}_2\text{O}$  products are compared in Figure 7 and it is seen that they are in overall quite good agreement.

**F. Velocity Scattering Angle Distribution and Comparison with Experiment.** 1.  $\text{OH}^- + \text{CH}_3\text{I} \rightarrow \text{CH}_3\text{OH} + \text{I}^-$ . The velocity scattering angle  $\theta$  is defined so that for  $\theta = 0^\circ$  the velocity vector of the  $\text{CH}_3\text{OH}$  product is pointing in the same direction as that for the  $\text{OH}^-$  reactant. For  $\theta = 180^\circ$  these vectors are pointing in opposite directions. The distributions of the velocity scattering angle, i.e., the scattering probability versus  $\cos(\theta)$ , obtained from the simulations are given in Figure 8 for the three atomic-level mechanisms. The distribution for the total scattering is given in Figure 9. The scattering for the direct stripping (DS) mechanism is in the forward direction with  $\cos(\theta)$  in the range 0.0–1.0. The scattering for the direct rebound (DR) mechanism is primarily in the backward direction with  $\cos(\theta)$  between  $-1.0$  and  $+0.20$ , with  $\cos(\theta)$  larger than 0.0 for a few trajectories. The indirect scattering covers the complete range of  $\cos(\theta)$ . The velocity scattering angles are concentrated in the forward directions for the three highest collision energies. For  $E_{\text{rel}}$  of 2.0 eV, the value of  $\cos(\theta)$  is most populated within the range of 0.6–0.9. This range extends to 0.5–1.0 for  $E_{\text{rel}}$  of 1.0 eV, and extends to 0.0–1.0 for  $E_{\text{rel}}$  of 0.5 eV. At  $E_{\text{rel}}$  of 0.05 eV, due to the increased fraction of the indirect mechanisms, the scattering is quite isotropic.

These velocity scattering angle distributions can be anticipated from the probabilities of the different mechanisms versus impact parameter  $b$ , as discussed in section IV.B and as displayed in Figure 3, which show the preference of DS for large  $b$  and the preference for DR for lower  $b$ . On the other hand, the indirect mechanisms, which may involve roundabout or formation of the prereaction complex, lead to more random distributions in comparison to the direct mechanism. Hence, the forms of the velocity scattering angle distributions follow the expected trends.

The total velocity scattering angle distributions for the  $\text{CH}_3\text{I} + \text{OH}^- \rightarrow \text{CH}_3\text{OH} + \text{I}^-$  reaction are compared with those measured experimentally in Figure 9. In the simulations forward scattering, i.e.,  $\cos(\theta)$  close to 1, dominates for the three largest  $E_{\text{rel}}$ . Though the experimental distributions for these  $E_{\text{rel}}$  have increased scattering for  $\cos(\theta) \sim 1$ , overall the distributions curves are quite flat and close to isotropic. The best agreement with simulation and experiment is for  $E_{\text{rel}} = 0.5 \text{ eV}$ . The simulation distribution is approximately isotropic at  $E_{\text{rel}}$  of 0.05 eV as a result of the importance of the indirect scattering.

2.  $\text{OH}^- + \text{CH}_3\text{I} \rightarrow \text{CH}_2\text{I}^- + \text{H}_2\text{O}$ . Similarly to the above  $\text{S}_{\text{N}}2$  pathway, the velocity scattering angle  $\theta$  is defined so that for  $\theta = 0^\circ$  the velocity vector of the  $\text{H}_2\text{O}$  product is pointing in the same direction as that for the  $\text{OH}^-$  reactant. For  $\theta = 180^\circ$  these vectors are pointing in opposite directions. The simulation distributions of the velocity scattering angle for this proton-transfer pathway are given in Figure 10 for the three atomic-level mechanisms. The scattering for  $\text{CH}_2\text{I}^- + \text{H}_2\text{O}$  is backward

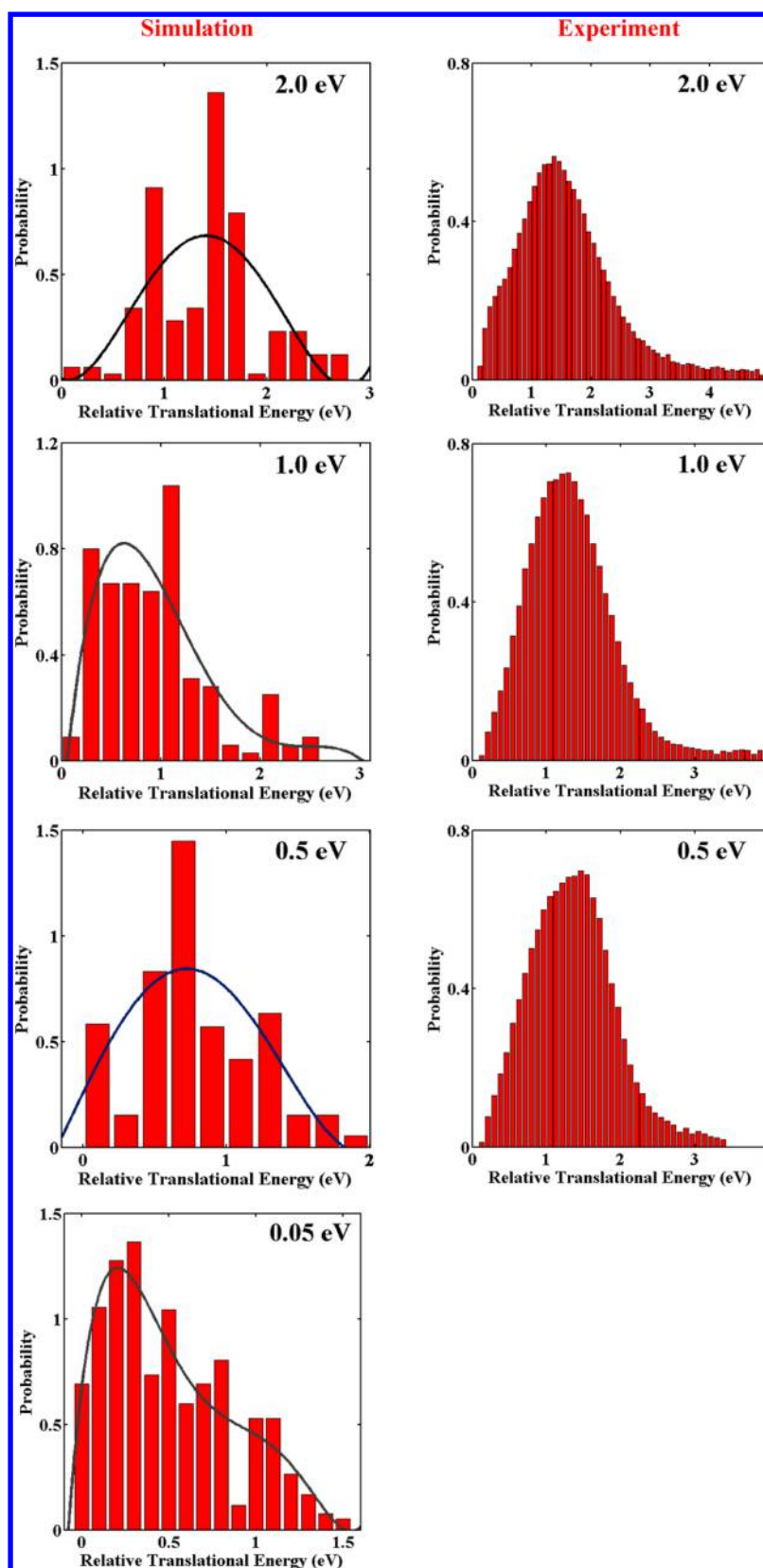


**Figure 6.** Comparison of simulation (left panel) and experimental (right panel) product relative translational energy distributions for the  $\text{CH}_3\text{OH} + \text{I}^-$  product pathway. The solid black curves are polynomial fits for the simulation distributions. The experimental distributions were determined from the ion images reported in refs 19 and 31.

and forward, respectively, for the direct rebound and direct stripping mechanism, and nearly isotropic for the indirect

mechanisms. The total velocity scattering angle distribution is given in Figure 11 and for  $E_{\text{rel}}$  of 2.0, 1.0, and 0.5 eV the

Table 7. Average Fractions of  $\text{OH}^- + \text{CH}_3\text{I} \rightarrow \text{CH}_2\text{I}^- + \text{H}_2\text{O}$  Product Energy Partitioning<sup>a</sup>

	$f_{\text{rel}}'$	$\text{CH}_2\text{I}^-$		$\text{H}_2\text{O}$	
		$f_{\text{rot}}'$	$f_{\text{vib}}'$	$f_{\text{rot}}'$	$f_{\text{vib}}'$
			$E_{\text{rel}} = 2.0 \text{ eV}$		
total	$0.71 \pm 0.03$	$0.14 \pm 0.01$	$0.05 \pm 0.01$	$0.06 \pm 0.01$	$0.04 \pm 0.02$
exp	$0.60 \pm 0.04$				
			$E_{\text{rel}} = 1.5 \text{ eV}$		
exp	$0.56 \pm 0.05$				
			$E_{\text{rel}} = 1.0 \text{ eV}$		
total	$0.54 \pm 0.02$	$0.28 \pm 0.01$	$0.11 \pm 0.01$	$0.06 \pm 0.01$	$0.01 \pm 0.01$
exp	$0.47 \pm 0.09$				
			$E_{\text{rel}} = 0.5 \text{ eV}$		
total	$0.49 \pm 0.04$	$0.25 \pm 0.02$	$0.15 \pm 0.01$	$0.07 \pm 0.01$	$0.04 \pm 0.01$
exp	$0.52 \pm 0.14$				
			$E_{\text{rel}} = 0.05 \text{ eV}$		
total	$0.38 \pm 0.03$	$0.20 \pm 0.02$	$0.21 \pm 0.02$	$0.14 \pm 0.01$	$0.07 \pm 0.01$

<sup>a</sup>The  $f$ 's are fractions of energy partitioning for relative translational, rotational, and vibrational energy. Total is the combined energy partitioning for all the atomic-level mechanisms. The B97-1/ECP/d harmonic ZPE was removed from the vibrational energy of the simulation results.  $f_{\text{rel}}'$  plus the total internal energy of  $\text{CH}_2\text{I}^-$  and  $\text{H}_2\text{O}$  equals unity.

scattering is strongly directed in the forward direction, as a result of the dominance of the direct stripping mechanism. At  $E_{\text{rel}}$  of 0.05 eV the overall scattering is approximately isotropic. The simulation and experimental velocity scattering angle distributions are compared in Figure 11. They are in excellent agreement for  $E_{\text{rel}}$  of 2.0 and 1.0 eV, but at 0.5 eV the simulation distribution is more strongly peaked at for  $\theta = 0^\circ$  than found in the experiments.

**G. Comparison with the  $\text{F}^- + \text{CH}_3\text{I}$  Simulations.** Because the  $\text{OH}^-$  and  $\text{F}^-$  ions are isoelectronic, it is of interest to compare their reactions with  $\text{CH}_3\text{I}$ . In previous work electronic structure calculations were performed to study the potential energy surface for the  $\text{F}^- + \text{CH}_3\text{I}$  reaction,<sup>29</sup> and direct dynamics were used to simulate the  $\text{F}^- + \text{CH}_3\text{I}$  reaction dynamics and compare with experiment.<sup>18,61</sup> The direct dynamics were performed with the DFT/B97-1/ECP/d method, the same approach used here for the  $\text{OH}^- + \text{CH}_3\text{I}$  direct dynamics. An important difference between these two systems, is the more complex reaction dynamics for  $\text{OH}^- + \text{CH}_3\text{I}$ . For  $\text{F}^- + \text{CH}_3\text{I}$  there are only two pathways, i.e., the  $\text{S}_{\text{N}}2$  products  $\text{CH}_3\text{F} + \text{I}^-$  and the proton-transfer products  $\text{CH}_2\text{I}^- + \text{HF}$ . However,  $\text{OH}^- + \text{CH}_3\text{I}$  has three additional pathways, reactions 4–6. Both the  $\text{F}^- + \text{CH}_3\text{I} \rightarrow \text{CH}_3\text{F} + \text{I}^-$  and  $\text{OH}^- + \text{CH}_3\text{I} \rightarrow \text{CH}_3\text{OH} + \text{I}^-$   $\text{S}_{\text{N}}2$  reactions are highly exothermic, with B97-1/ECP/d classical potential energy release values of  $-46.7$  and  $-68.8$  kcal/mol, respectively. They have similar  $\text{F}^- \cdots \text{HCH}_2\text{I}$  and  $\text{OH}^- \cdots \text{HCH}_2\text{I}$  hydrogen-bonded prereaction complexes with respective classical potential energies of  $-20.2$  and  $-20.1$ . The energy barriers between these  $\text{C}_s$  prereaction complexes and their  $\text{S}_{\text{N}}2$  transition states are very low, 2.4 kcal/mol for the  $\text{F}^-$  reaction and 1.3 kcal/mol for the  $\text{OH}^-$  reaction. Their postreaction complex is quite different. It is a  $\text{C}_{3v}$   $\text{FCH}_3 \cdots \text{I}^-$  complex for the  $\text{F}^- + \text{CH}_3\text{I}$  reaction, but a  $\text{C}_s$   $\text{I}^- \cdots \text{HOCH}_3$  hydrogen-bonded complex for the  $\text{OH}^- + \text{CH}_3\text{I}$  reaction.

Direct dynamics simulations were performed at 0.32 and 1.53 eV for the  $\text{F}^- + \text{CH}_3\text{I}$  reaction,<sup>18,61</sup> and these simulation results may be compared with the current results for the  $\text{OH}^- + \text{CH}_3\text{I}$  reaction at  $E_{\text{rel}}$  of 0.5, 1.0, and 2.0 eV. For the  $\text{S}_{\text{N}}2$  pathway, the  $\text{F}^- + \text{CH}_3\text{I}$  reaction has a cross section of 109 and  $9 \text{ \AA}^2$  at  $E_{\text{rel}}$  of 0.32 and 1.53 eV, respectively. For the  $\text{OH}^- + \text{CH}_3\text{I}$  reaction at  $E_{\text{rel}}$  of 0.5, 1.0, and 2.0 eV, the respective  $\text{S}_{\text{N}}2$  cross sections are 17, 11, and  $4 \text{ \AA}^2$ . The  $\text{F}^-$  and  $\text{OH}^-$  reactions have similar  $\text{S}_{\text{N}}2$

cross sections at high  $E_{\text{rel}}$ , but for lower  $E_{\text{rel}}$  the  $\text{F}^-$  reaction has a larger cross section (as given in Table 4, for the quite low  $E_{\text{rel}}$  of 0.05 eV the  $\text{OH}^- \text{S}_{\text{N}}2$  cross section is only  $76 \text{ \AA}^2$ ). For the  $\text{F}^- + \text{CH}_3\text{I}$  reaction, proton transfer to form  $\text{CH}_2\text{I}^- + \text{HF}$  only occurred at 1.53 eV with a cross section of  $2.1 \text{ \AA}^2$ . In contrast, for the  $\text{OH}^- + \text{CH}_3\text{I}$  reaction, proton transfer occurs at each  $E_{\text{rel}}$  with cross sections of 38, 18, and  $9 \text{ \AA}^2$  for  $E_{\text{rel}}$  of 0.5, 1.0, and 2.0 eV, respectively.

Both the  $\text{OH}^- + \text{CH}_3\text{I}$  and  $\text{F}^- + \text{CH}_3\text{I}$   $\text{S}_{\text{N}}2$  reactions have direct and indirect mechanisms, with the same direct stripping and direct rebound mechanisms. For the  $\text{OH}^- + \text{CH}_3\text{I}$   $\text{S}_{\text{N}}2$  reaction, the respective percentages for the direct rebound, direct stripping, and indirect mechanisms are 30%, 65%, and 5%; 18%, 63% and 19%; 23%, 35%, and 42%; and 33%, 28%, and 39% for  $E_{\text{rel}}$  of 2.0, 1.0, 0.5, and 0.05 eV, respectively. For the  $\text{F}^- + \text{CH}_3\text{I}$   $\text{S}_{\text{N}}2$  reaction these respective percentages are 29%, 12%, and 59%; and 15%, 25%, and 60% for  $E_{\text{rel}}$  of 1.53 and 0.32 eV, respectively. In comparing the atomic-level mechanisms for these two  $\text{S}_{\text{N}}2$  reactions, the indirect reactions are most important for the  $\text{F}^- + \text{CH}_3\text{I}$  reaction, whereas the direct stripping reaction is most important for the  $\text{OH}^- + \text{CH}_3\text{I}$  reaction at high collision energy with the indirect reactions becoming most important at lower collision energies.

The two  $\text{S}_{\text{N}}2$  reactions share several atomic-level indirect mechanisms, which are formation of the hydrogen-bonded prereaction complex ( $\text{F}^- \cdots \text{HCH}_2\text{I}$  or  $\text{HO}^- \cdots \text{HCH}_2\text{I}$ ), recrossing of the central barrier ( $[\text{F}^- \cdots \text{HCH}_2\text{I}]^-$  or  $[\text{HO}^- \cdots \text{HCH}_2\text{I}]^-$ ), the roundabout mechanism, and combinations of them. Though formation of the prereaction complex is the most important indirect mechanism for both  $\text{S}_{\text{N}}2$  reactions, it is more important for  $\text{F}^- + \text{CH}_3\text{I} \rightarrow \text{CH}_3\text{F} + \text{I}^-$ , for which 58% involved formation of the prereaction complex for  $E_{\text{rel}}$  of both 0.32 and 1.53 eV. For  $\text{OH}^- + \text{CH}_3\text{I} \rightarrow \text{CH}_3\text{OH} + \text{I}^-$ , this percentage is 36% (0.05 eV), 38% (0.5 eV), and 14% (1.0 eV). For the  $\text{F}^- + \text{CH}_3\text{I} \rightarrow \text{CH}_3\text{F} + \text{I}^-$  reaction a small percentage of the indirect mechanisms involved forming the  $\text{C}_{3v}$   $\text{FCH}_3 \cdots \text{I}^-$  postreaction complex, i.e., 4% and 1% at  $E_{\text{rel}}$  of 0.32 and 1.53 eV, respectively. On the contrary, formation of the  $\text{C}_s$   $\text{I}^- \cdots \text{HOCH}_3$  postreaction complex was not observed in the  $\text{OH}^- + \text{CH}_3\text{I}$  simulations. Two new indirect mechanisms, called proton exchange and proton exchange rotation, were identified for the  $\text{OH}^- + \text{CH}_3\text{I} \rightarrow \text{CH}_3\text{OH} + \text{I}^-$  reaction.

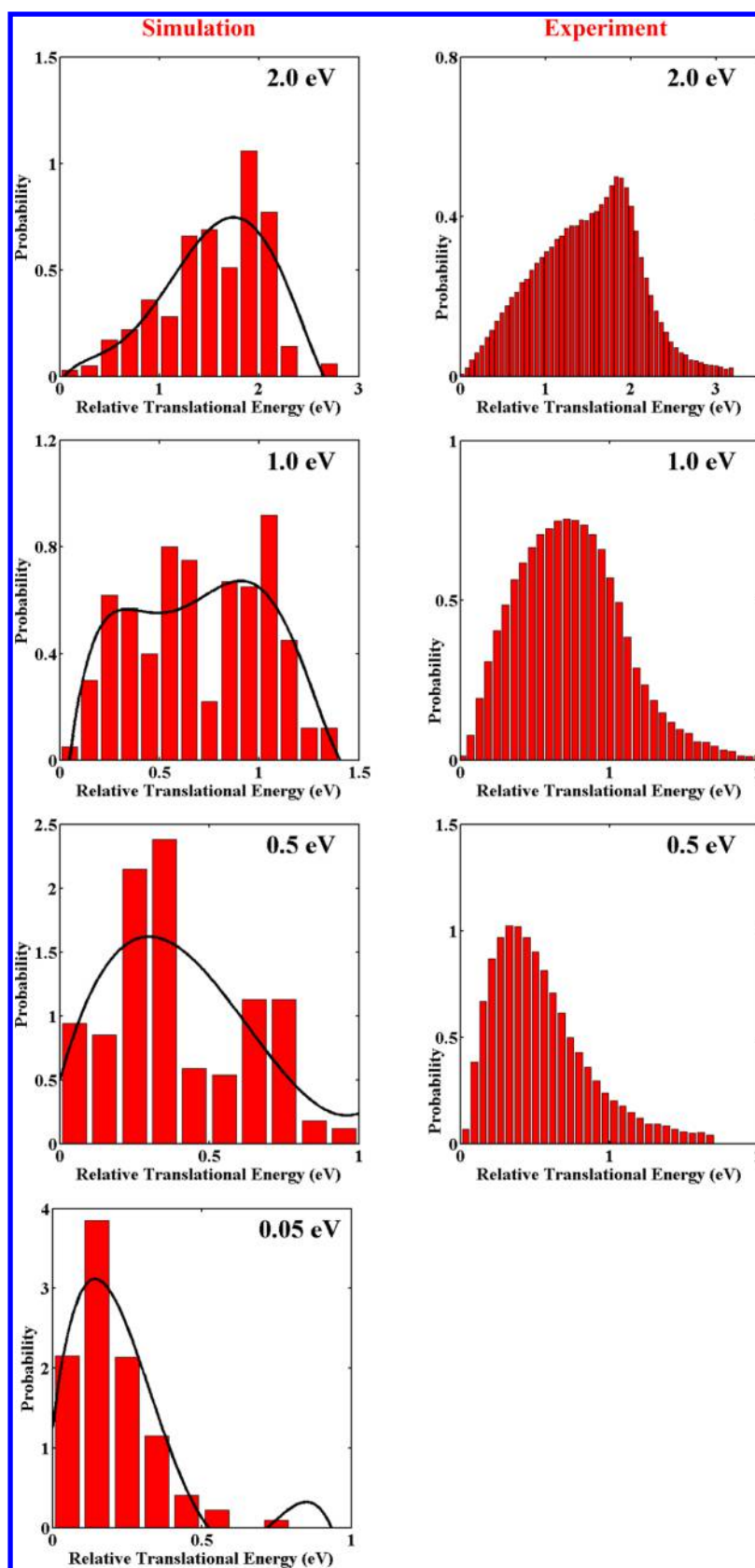


**Figure 7.** Comparison of simulation (left panel) and experimental (right panel) product relative translational energy distributions for the  $\text{CH}_2\text{I}^- + \text{H}_2\text{O}$  product pathway. The solid black curves are polynomial fits for the simulation distributions. The experimental distributions were determined from the ion images reported in refs 19 and 31.

There are both similarities and differences in the product energy partitioning for the two  $\text{S}_{\text{N}}2$  reactions. For both the

majority of the energy is partitioned to product internal degrees of freedom, with similar  $f_{\text{int}}'$  for the two reactions. The fraction

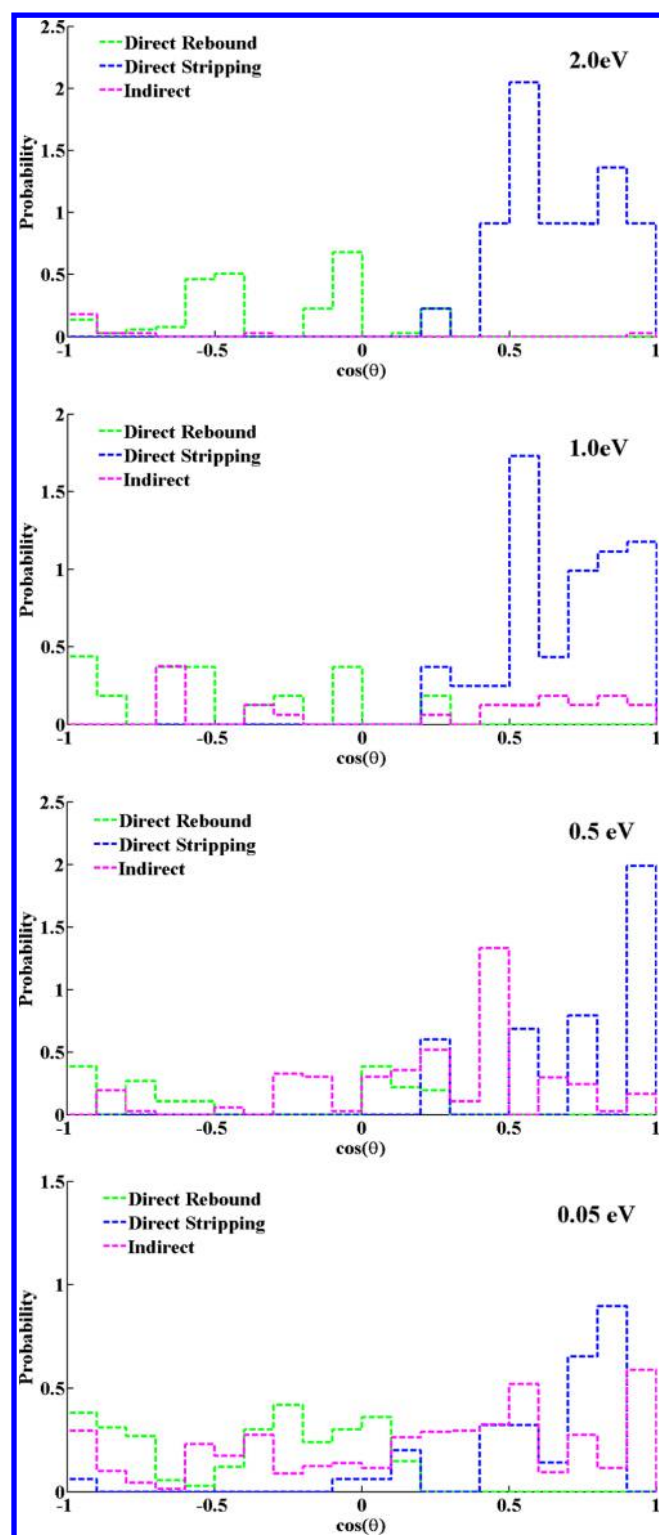


**Figure 8.** Distribution of the velocity scattering angle for different atomic-level mechanisms for the  $\text{CH}_3\text{OH} + \text{I}^-$  product angle pathway at the different  $E_{\text{rel}}$ . Distributions are given for the direct rebound (green), direct stripping (blue), and indirect (pink) atomic-level mechanisms.

$f_{\text{int}}'$  equals  $0.69 \pm 0.02$  for  $\text{F}^- + \text{CH}_3\text{I}$  at  $E_{\text{rel}} = 0.32$  eV and  $0.75 \pm 0.02$  for  $\text{OH}^- + \text{CH}_3\text{I}$  at  $E_{\text{rel}} = 0.5$  eV. At the higher collision energies  $f_{\text{int}}'$  equals  $0.63 \pm 0.04$  for  $\text{F}^- + \text{CH}_3\text{I}$  at  $E_{\text{rel}} = 1.53$  eV, and  $0.76 \pm 0.02$  and  $0.68 \pm 0.02$  for  $\text{OH}^- + \text{CH}_3\text{I}$  at  $E_{\text{rel}}$  of 1.0 and 2.0 eV, respectively. The product energy partitionings for the two reactions are similar for both the indirect reactions and

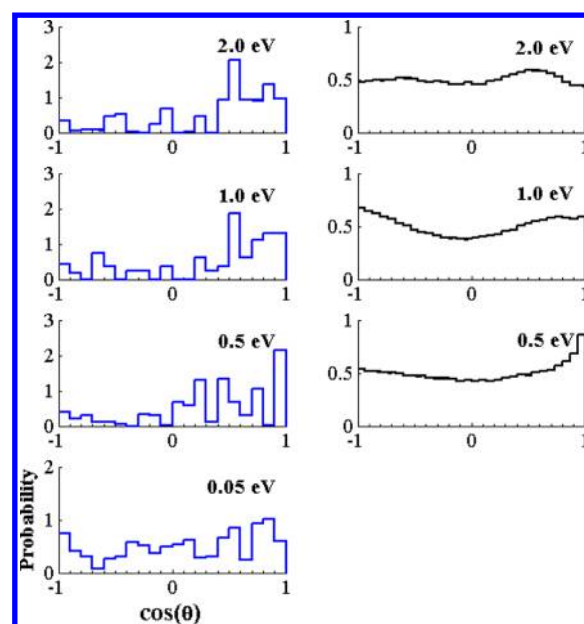


**Figure 9.** Comparison of velocity scattering angles distributions for the  $\text{CH}_3\text{OH} + \text{I}^-$  pathway between simulations (left panel) and experiments (right panel). The experimental distributions were determined from the ion images reported in refs 19 and 31.

the direct stripping reaction. However, the energy partitioning is decidedly different for the direct rebound mechanism, with  $f_{\text{rel}}'$  smaller for  $\text{OH}^- + \text{CH}_3\text{I}$  as a result more energy transfer to  $\text{CH}_3\text{OH}$  vibration for this reaction.

Each atomic-level  $\text{S}_{\text{N}}2$  reaction mechanism has a similar velocity scattering angle distribution for  $\text{F}^- + \text{CH}_3\text{I} \rightarrow \text{CH}_3\text{F} + \text{I}^-$  and  $\text{OH}^- + \text{CH}_3\text{I} \rightarrow \text{CH}_3\text{OH} + \text{I}^-$ . The scattering for the direct rebound and direct stripping mechanisms is primarily in the backward and forward directions, respectively. On the other hand, the scattering for the indirect mechanisms is approximately isotropic.

## V. SUMMARY

Direct dynamics simulations at the B97-1/ECP/d level of theory were performed to study the atomic-level dynamics for the  $\text{OH}^- + \text{CH}_3\text{I}$  reaction and compare with experiment. This electronic structure method gives reaction energetics in good agreement with high-level calculations and experiment. The simulations were performed for collision energies of 2.0, 1.0, 0.5, and 0.05 eV. The following are the important findings from the simulations.

Concerning the reaction pathways and their atomistic mechanisms:

- (1) Five different pathways are observed in the simulations, forming  $\text{CH}_3\text{OH} + \text{I}^-$ ,  $\text{CH}_2\text{I}^- + \text{H}_2\text{O}$ ,  $\text{CH}_2 + \text{I}^- + \text{H}_2\text{O}$ ,  $\text{IOH}^- + \text{CH}_3$ , and  $[\text{CH}_3\text{-I-OH}]^-$ . The first two pathways, i.e.,  $\text{S}_{\text{N}}2$  and proton transfer, dominate the reaction dynamics. Though the  $\text{S}_{\text{N}}2$  reaction is barrierless with a large exothermicity of  $-64.9$  kcal/mol, the cross section for proton transfer which has a reaction exothermicity of  $-4.2$  kcal/mol has the larger cross section except for the smallest collision energy of 0.05 eV.
- (2) The  $\text{S}_{\text{N}}2$  and proton-transfer pathways have direct rebound, direct stripping, and indirect reaction mechanisms. Direct rebound and stripping have velocity

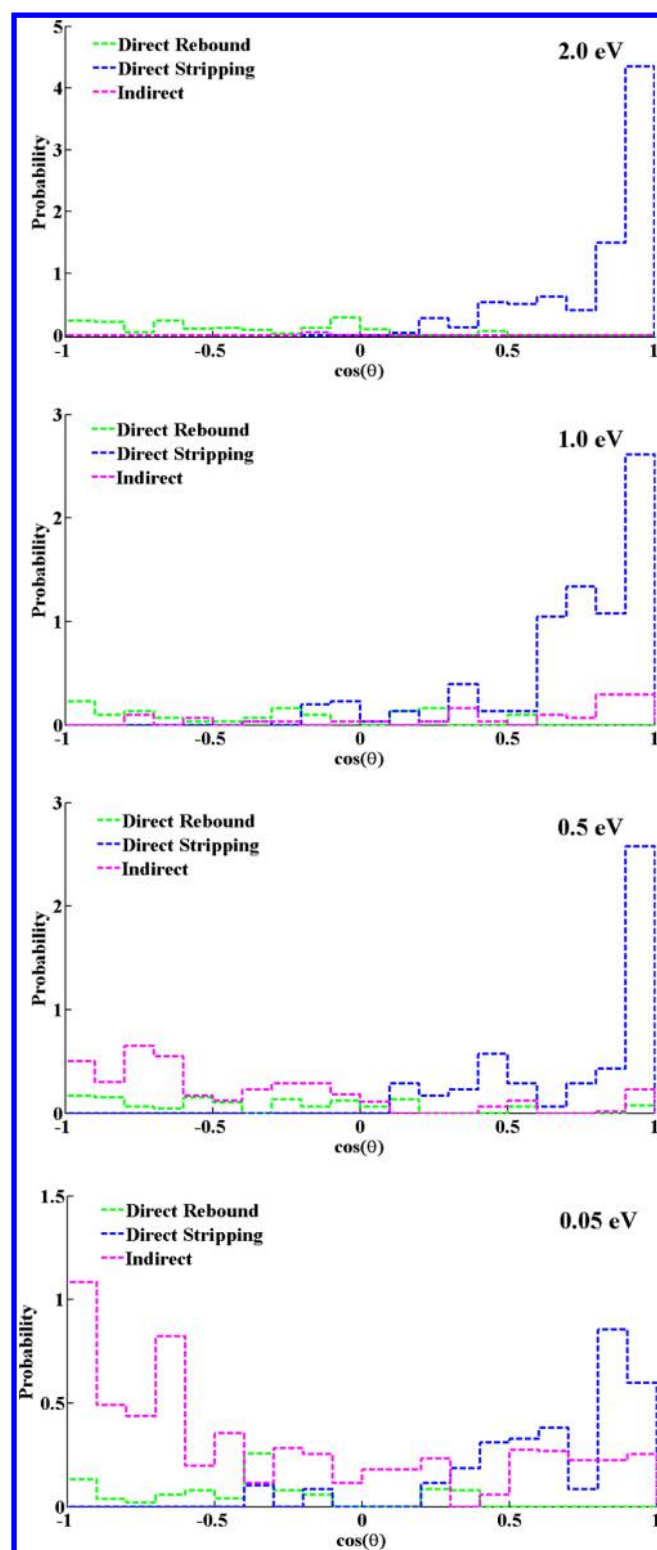


**Figure 10.** Simulation distribution of velocity scattering angles  $\text{CH}_2\text{I}^- + \text{H}_2\text{O}$  pathway at  $E_{\text{rel}}$  of 2.0, 1.0, 0.5, and 0.05 eV. Distributions are given for the direct rebound (green), direct stripping (blue), and indirect (pink) atomic-level mechanisms.

scattering angles in the backward and forward directions, respectively, whereas the scattering is approximately isotropic for the indirect reactions. For the  $\text{S}_{\text{N}}2$  pathway, direct reaction dominates at all collision energies, with stripping more important than rebound except for the

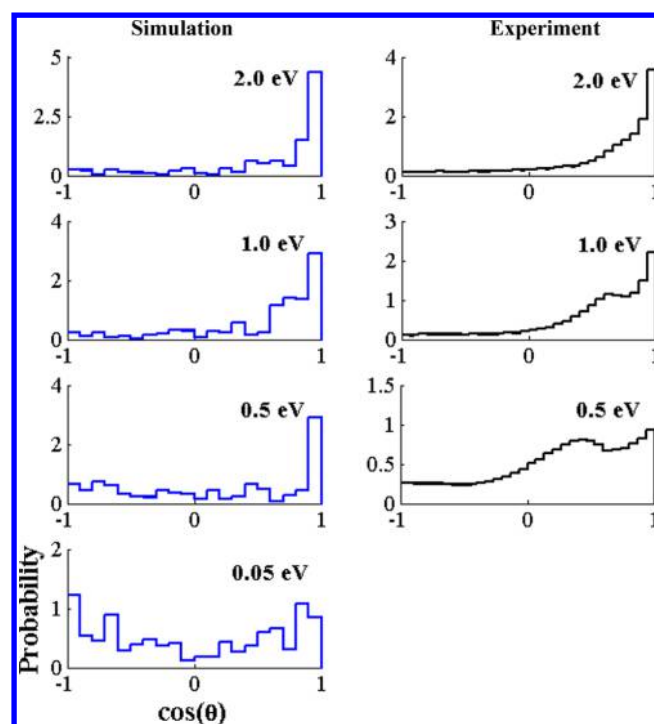


**Figure 11.** Comparison of velocity scattering angles distributions for the  $\text{CH}_2\text{I}^- + \text{H}_2\text{O}$  pathway between simulations (left panel) and experiments (right panel). The experimental distributions were determined from the ion images reported in refs 19 and 31.

lowest collision energy. At 0.5 and 0.05 eV, the indirect reactions are more important than either rebound or stripping. For the proton-transfer pathway, stripping is much more important than rebound at all collision energies. Stripping is the dominant mechanism at 2.0, 1.0, and 0.5 eV, where direct reaction is more important than indirect. The majority of the reaction is indirect at 0.05 eV.

- (3) Indirect reaction for the  $\text{S}_{\text{N}}2$  pathway occurs by several different atomistic mechanisms. At 2.0 eV the only indirect process is the roundabout mechanism. At the other collision energies, 70–90% of the indirect reaction for the  $\text{S}_{\text{N}}2$  pathway occurs by forming the  $\text{OH}^- \cdots \text{HCH}_2\text{I}$  hydrogen-bonded prereaction complex. There are three important indirect mechanisms for the proton-transfer pathway, i.e., the roundabout, formation of the hydrogen-bonded prereaction complex, formation of the  $\text{CH}_2\text{I}^- \cdots \text{HOH}$  complex, and couplings between these mechanisms. At 2.0 eV all of the indirect reaction occurs by the roundabout mechanism and at 1.0 eV the roundabout's contribution is 75%. At 0.5 eV the majority of the indirect reaction occurs via the hydrogen-bonded prereaction complex. At 0.05 eV, mechanisms with the hydrogen-bonded prereaction complex and the  $\text{CH}_2\text{I}^- \cdots \text{HOH}$  complex contribute 96% of the indirect reaction, with the latter the most important. There is considerable richness in the detail of the indirect mechanisms for the  $\text{OH}^- + \text{CH}_3\text{I}$  reaction.
- (4) Though the hydrogen-bonded postreaction complex  $\text{CH}_3\text{OH} \cdots \text{I}^-$  is a potential minimum on the  $\text{S}_{\text{N}}2$  reaction pathway, this complex was not formed in the simulations for  $E_{\text{rel}}$  of 0.05 to 2.0 eV. Accessing this complex is barrierless in the exit-channel and the trajectories either

pass through<sup>20</sup> or pass by<sup>30</sup> this minimum. The latter was observed in both experiments<sup>64</sup> and simulations<sup>65</sup> of the  $F^- + CH_3OOH$  reaction. In a simulation study<sup>30</sup> of the  $OH^- + CH_3F$  reaction ~20% of the trajectories formed the  $CH_3OH\cdots F^-$  postreaction complex. Because the  $CH_3OH\cdots F^-$  and  $CH_3OH\cdots I^-$  complexes are similar, it is interesting that the latter is not formed in the current study for which there are several reasons. The potential energy minimum is deeper for  $CH_3OH\cdots F^-$  than  $CH_3OH\cdots I^-$ , which should enhance the formation of the former complex. In addition, for the  $OH^- + CH_3F$  simulation study the trajectories were initialized at the  $S_N2$  central barrier with 300 K rotational and vibrational energies. The energy at the  $S_N2$  barrier is higher for the current study because the trajectories are initialized at the  $OH^- + CH_3I$  reactants, which has a higher potential energy than that at the central barrier (Figure 1). Also, the angular momentum of the reactive system is higher for the current simulation. Both the higher energy and angular momentum may promote direction reaction from the  $S_N2$  barrier to the  $CH_3OH + I^-$  products, without forming the postreaction complex.

Concerning product energy partitioning:

- (5) The energy of the  $CH_3OH + I^-$   $S_N2$  products is preferentially partitioned to  $CH_3OH$  internal energy with  $f_{int}' \sim 0.70$  for the higher three  $E_{rel}$ , but larger and 0.80 for  $E_{rel} = 0.05$  eV. The latter results from the increased importance of indirect reaction at 0.05 eV, which enhances energy transfer to  $CH_3OH$  vibration. Energy transfer to vibration increases with decrease in  $E_{rel}$  for both the direct rebound and stripping pathways, but their largest  $f_{vib}'$  is 0.66 and  $f_{vib}'$  is always larger for the indirect reactions. At each  $E_{rel}$ , stripping transfers more energy to  $CH_3OH$  vibration than does rebound. For the higher two  $E_{rel}$ , stripping transfers more energy to  $CH_3OH$  rotation than does rebound, but the opposite is the case for the lower two  $E_{rel}$ . The  $OH^- + CH_3I \rightarrow CH_3OH + I^-$  total product energy partitioning and that for the individual reaction mechanisms are similar to those for the isoelectronic  $F^- + CH_3I \rightarrow CH_3F + I^-$  reaction.<sup>18,61</sup>
- (6) The energy of the  $CH_2I^- + H_2O$  proton-transfer products is preferentially partitioned to relative translation at  $E_{rel} = 2.0$  eV with  $f_{rel}' = 0.71$ , but to product internal energies at  $E_{rel} = 0.05$  eV with  $f_{rel}'$  much smaller and equal to 0.38. At  $E_{rel} = 0.5$  eV the transfer to product relative translation and internal energies are equal. The internal energy of  $CH_2I^-$  is much larger than that for  $H_2O$ , with the rotational energy of  $CH_2I^-$  two to three times larger than its vibrational energy.

Concerning comparison with experiment:

- (7) There is overall quite good agreement between the simulations and experiments. The same product ions are observed for both, i.e.,  $I^-$ ,  $CH_2I^-$ , and  $IOH^-$ , with  $I^-$  and  $CH_2I^-$  comprising 98% or more of the product ions. The simulation and experimental ratios of the product ions are in excellent agreement at  $E_{rel}$  of 2.0 and 1.0 eV. However, at 0.5 eV they are different with an  $I^-:CH_2I^-$  ratio of 0.31:0.69 in the simulations and 0.56:0.44 in the experiments. The simulation and experimental product energy partitioning, including the relative translational energy distribution, are in good agreement for the  $OH^- + CH_3I$   $S_N2$  pathway. The same is found for the proton-

transfer pathway, except for  $E_{rel} = 2.0$  eV where the simulation finds more energy transfer to product relative translation than for the experiments, i.e.,  $f_{rel}' = 0.71 \pm 0.03$  for the simulations in comparison to 0.60 for the experiments. There is good agreement between the simulation and experimental relative velocity scattering angle distributions for the proton-transfer pathway, but not for the  $S_N2$  pathway. For the latter the experimental distributions for the different  $E_{rel}$  are isotropic in nature, whereas those for the simulations are peaked in the forward direction as a result larger fraction of direct stripping versus direct rebound.

The  $[CH_3\cdots I\cdots OH]^-$  intermediate is observed in the simulations and at the lowest collision energies some of them remain when the trajectories are terminated. They would dissociate if the trajectories were calculated for a longer time. This intermediate is not observed experimentally.

Concerning accuracy of the direct dynamics simulations:

- (8) The accuracy of the direct dynamics simulations depends upon the accuracy of the quasiclassical trajectory method and the electronic structure theory used for the simulations. A detailed discussion of the accuracy of the quasiclassical trajectory method for simulating the dynamics of  $X^- + CH_3Y$  reactions was considered in recent reviews.<sup>6,62</sup> For direct reactions, without trapping in long-lived intermediates, the trajectories are expected to give accurate results. For long-lived intermediates, the unphysical flow of zero-point energy (ZPE) may lead to inaccurate reaction dynamics.<sup>63</sup> For the  $OH^- + CH_3I$  reaction this is expected to be most important at low collision energies where indirect reactions and intermediates participate more predominately, an effect that may be particularly important for endothermic and thermoneutral reactions. Such an incorrect treatment of ZPE may explain the smaller  $I^-:CH_2I^-$  ratio in the simulations as compared to experiment for the 0.5 eV collisions. Indirect reaction, with formation of the  $OH^-\cdots HCH_2I$  prereaction complex, is important at this collision energy and the incorrect treatment of ZPE may enhance the formation of the nearly thermoneutral  $CH_2I^- + H_2O$  proton-transfer products. The two remaining differences between simulation and experiment suggest inaccuracies in the B97-1/ECP/d electronic structure theory used to represent the PES for the simulations. The principal difference between the product energy partitioning for the simulations and experiments is for the proton-transfer pathway and  $E_{rel} = 2.0$  eV, where the reaction is primarily direct and the possible problem with ZPE should not be important. Also, the simulation and experimental relative velocity scattering angle distributions for the  $S_N2$  pathway are different at all collision energies, suggestive of inaccuracies in the B97-1/ECP/d PES. The implication from this comparison is that the B97-1 PES leads to more reaction by stripping as compared to experiment. Though the B97-1 PES gives quite accurate energetics for the  $OH^- + CH_3I$  reaction and accurately represents many of the reaction dynamics, in future work it will be important to consider additional electronic structure theory methods in direct dynamics simulations of the reaction dynamics.

## AUTHOR INFORMATION

## Notes

The authors declare no competing financial interest.

## ACKNOWLEDGMENTS

The direct chemical dynamics simulations reported here are based upon work supported by the National Science Foundation under Grants No. CHE-0957521 and the Robert A. Welch Foundation under Grant No. D-0005. Support was also provided by the High-Performance Computing Center (HPCC) at Texas Tech University, under the direction of Philip W. Smith and the Texas Advanced Computing Center (TACC) at the University of Texas at Austin. The experimental work was supported by the Deutsche Forschungsgemeinschaft under contract No. WE2592/3-2. R.O. acknowledges support by the Landesgraduiertenförderung Baden-Württemberg. We thank the University of Freiburg, where the measurements presented here have been carried out, for supporting this research.

## REFERENCES

- (1) Farneth, W. E.; Brauman, J. I. Dynamics of Proton Transfer Involving Delocalized Negative Ions in the Gas Phase. *J. Am. Chem. Soc.* **1976**, *98*, 7891–7898.
- (2) Hase, W. L. Simulation of Gas-Phase Chemical Reactions: Applications to  $S_N2$  Nucleophilic Substitution. *Science* **1994**, *266*, 998–1002.
- (3) (a) O'Hair, R. A. J.; Davico, G. E.; Hacaloglu, J.; Dang, T. T.; Dupuy, C. H.; Bierbaum, V. M. Measurements of Solvent and Secondary Kinetic Isotope Effects for the Gas Phase  $S_N2$  Reactions of Fluoride with Methyl Halides. *J. Am. Chem. Soc.* **1994**, *116*, 3609–3610. (b) Garver, J. M.; Gronert, S.; Bierbaum, V. M. Experimental Validation of the  $\alpha$ -Effect in the Gas Phase. *J. Am. Chem. Soc.* **2011**, *133*, 13894–13897.
- (4) Chabinyk, M. L.; Craig, S. L.; Regan, C. K.; Brauman, J. I. Gas-Phase Ionic Reactions: Dynamics and Mechanism of Nucleophilic Displacements. *Science* **1998**, *279*, 1882–1886.
- (5) Laerdahl, J. K.; Uggerud, E. Gas Phase Nucleophilic Substitution. *Int. J. Mass Spectrom.* **2002**, *214*, 277–314.
- (6) Manikandan, P.; Zhang, J.; Hase, W. L. Chemical Dynamics Simulations of  $X^- + CH_3Y \rightarrow XCH_3 + Y^-$  Gas-Phase  $S_N2$  Nucleophilic Substitution Reactions. Non-Statistical Dynamics and Non-Traditional Reaction Mechanisms. *J. Phys. Chem. A* **2012**, *116*, 3061–3080.
- (7) Mikosch, J.; Weidemüller, M.; Wester, R. On the Dynamics of Chemical Reactions of Negative Ions. *Int. Rev. Phys. Chem.* **2010**, *29*, 589–617.
- (8) Mikosch, J. Dynamics of Anion-Molecule Reactions at Low Energy. *Ph.D. Dissertation*, Physikalisches Institut, Universität at Freiburg, Freiburg, Germany, 2007.
- (9) Viggiano, A. A.; Morris, R. A.; Paschkewitz, J. S.; Paulson, J. F. Kinetics of the Gas-Phase Reactions of Chloride Anion,  $Cl^-$  with  $CH_3Br$  and  $CD_3Br$ : Experimental Evidence for Nonstatistical Behavior? *J. Am. Chem. Soc.* **1992**, *114*, 10477–10482.
- (10) Li, C.; Ross, P.; Szulejko, J. E.; McMahon, T. B. High-Pressure Mass Spectrometric Investigations of the Potential Energy Surfaces of Gas-Phase  $S_N2$  Reactions. *J. Am. Chem. Soc.* **1996**, *118*, 9360–9367.
- (11) Craig, S. L.; Brauman, J. I. Phase-Shifting Acceleration of Ions in an Ion Cyclotron Resonance Spectrometer: Kinetic Energy Distribution and Reaction Dynamics. *J. Phys. Chem. A* **1997**, *101*, 4745–4752.
- (12) DeTuri, V. F.; Hintz, P. A.; Ervin, K. M. Translational Activation of the  $S_N2$  Nucleophilic Displacement Reactions  $Cl^- + CH_3Cl (CD_3Cl) \rightarrow ClCH_3 (ClCD_3) + Cl^-$ : A Guided Ion Beam Study. *J. Phys. Chem. A* **1997**, *101*, 5969–5986.
- (13) Tonner, D. S.; McMahon, T. B. Non-Statistical Effects in the Gas Phase  $S_N2$  Reaction. *J. Am. Chem. Soc.* **2000**, *122*, 8783–8784.
- (14) Wester, R.; Bragg, A. E.; Davis, A. V.; Neumark, D. M. Time-Resolved Study of the Symmetric  $S_N2$ -Reaction  $I^- + CH_3I$ . *J. Chem. Phys.* **2003**, *119*, 10032–10039.
- (15) Angel, L. A.; Ervin, K. M. Gas-Phase  $S_N2$  and Bromine Abstraction Reactions of Chloride Ion with Bromomethane: Reaction Cross Sections and Energy Disposal into Products. *J. Am. Chem. Soc.* **2003**, *125*, 1014–1027.
- (16) Mikosch, J.; Otto, R.; Trippel, S.; Eichhorn, C.; Weidemüller, M.; Wester, R. Inverse Temperature Dependent Lifetimes of Transient  $S_N2$  Ion-Dipole Complexes. *J. Phys. Chem. A* **2008**, *112*, 10448–10452.
- (17) Mikosch, J.; Trippel, S.; Eichhorn, C.; Otto, R.; Lourderaj, U.; Zhang, J. X.; Hase, W. L.; Weidemüller, M.; Wester, R. Imaging Nucleophilic Substitution Dynamics. *Science* **2008**, *319*, 183–186.
- (18) Zhang, J.; Mikosch, J.; Trippel, S.; Otto, R.; Weidemüller, M.; Wester, R.; Hase, W. L.  $F^- + CH_3I \rightarrow FCH_3 + I^-$  Reaction Dynamics. Non-Traditional Atomistic Mechanisms and Formation of a Hydrogen-Bonded Complex. *J. Phys. Chem. Lett.* **2010**, *1*, 2747–2752.
- (19) Otto, R.; Brox, J.; Stei, M.; Trippel, S.; Best, T.; Wester, R. Single Solvent Molecules can Affect the Dynamics of Substitution Reactions. *Nature Chem.* **2012**, *4*, 534–538.
- (20) Vande Linde, S. R.; Hase, W. L. A Direct Mechanism for  $S_N2$  Nucleophilic Substitution Enhanced by Mode Selective Vibrational Excitation. *J. Am. Chem. Soc.* **1989**, *111*, 2349–2351.
- (21) Vande Linde, S. R.; Hase, W. L. Trajectory Studies of  $S_N2$  Nucleophilic Substitution. I. Dynamics of  $Cl^- + CH_3Cl$  Reactive Collisions. *J. Chem. Phys.* **1990**, *93*, 7962–7980.
- (22) Cho, Y. J.; Vande Linde, S. R.; Zhu, L.; Hase, W. L. Trajectory Studies of  $S_N2$  Nucleophilic Substitution. II. Nonstatistical Central Barrier Recrossing in the  $Cl^- + CH_3Cl$  System. *J. Chem. Phys.* **1992**, *96*, 8275–8287.
- (23) Hase, W. L.; Cho, Y. J. Trajectory Studies of  $S_N2$  Nucleophilic Substitution. III. Dynamical Stereochemistry and Energy Transfer Pathways for the  $Cl^- + CH_3Cl$  Association and Direct Substitution Reactions. *J. Chem. Phys.* **1993**, *98*, 8626–8639.
- (24) Wang, H.; Peslherbe, G. H.; Hase, W. L. Trajectory Studies of  $S_N2$  Nucleophilic Substitution. IV. Intramolecular and Unimolecular Dynamics of the  $Cl^- - CH_3Br$  and  $ClCH_3 - Br^-$  Complexes. *J. Am. Chem. Soc.* **1994**, *116*, 9644–9651.
- (25) Peslherbe, G. H.; Wang, H.; Hase, W. L. Unimolecular Dynamics of  $Cl^- - CH_3Cl$  Intermolecular Complexes Formed by  $Cl^- + CH_3Cl$  Association. *J. Chem. Phys.* **1995**, *102*, 5626–5635.
- (26) Mann, D. J.; Hase, W. L. Trajectory Studies of  $S_N2$  Nucleophilic Substitution. 6. Translational Activation of the  $Cl^- + CH_3Cl$  Reaction. *J. Phys. Chem. A* **1998**, *102*, 6208–6214.
- (27) Sun, L.; Hase, W. L.; Song, K. Trajectory Studies of  $S_N2$  Nucleophilic Substitution. 8. Central Barrier Dynamics for Gas Phase  $Cl^- + CH_3Cl$ . *J. Am. Chem. Soc.* **2001**, *123*, 5753–5756.
- (28) Wang, Y.; Hase, W. L.; Wang, H. Trajectory Studies of  $S_N2$  Nucleophilic Substitution. 9. Microscopic Reaction Pathways and Chemical Kinetics for  $Cl^- + CH_3Br$ . *J. Chem. Phys.* **2003**, *118*, 2688–2695.
- (29) Zhang, J.; Hase, W. L. Electronic Structure Theory Study of the  $F^- + CH_3I \rightarrow FCH_3 + I^-$  Potential Energy Surface. *J. Phys. Chem. A* **2010**, *114*, 9635–9643.
- (30) Sun, L.; Song, K.; Hase, W. L. A  $S_N2$  Reaction that Avoids Its Deep Potential Energy Minimum. *Science* **2002**, *296*, 875–878.
- (31) Otto, R.; Xie, J.; Brox, J.; Trippel, S.; Stei, M.; Best, T.; Siebert, M. R.; Hase, W. L.; Wester, R. Reaction Dynamics of Temperature-Variable Anion Water Clusters Studied with Crossed Beams and by Direct Dynamics. *Faraday Discuss.* **2012**, *157*, 41–57.
- (32) Bylaska, E. J.; de Jong, W. A.; Govind, N.; Kowalski, K.; Straatsma, T. P.; Valiev, M.; Wang, D.; Apra, E.; Windus, T. L.; Hammond, J.; et al. *NWChem, A Computational Chemistry Package for Parallel Computers*, Version 5.1; Pacific Northwest National Laboratory: Richland, Washington 99352-0999, USA, 2007.
- (33) Kendall, R. A.; Apra, E.; Bernholdt, D. E.; Bylaska, E. J.; Dupuis, M.; Fann, G. I.; Harrison, R. J.; Ju, J.; Nichols, J. A.; Nieplocha, J.; et al. High Performance Computational Chemistry: An Overview of

NWChem a Distributed Parallel Application. *Comput. Phys. Commun.* **2000**, *128*, 260–283.

(34) Hehre, W. J.; Radom, L.; Schleyer, P. V. R.; Pople, J. A. *Ab Initio Molecular Orbital Theory*; Wiley: New York, 1986.

(35) Parr, R. G.; Yang, W. *Density Functional Theory of Atoms and Molecules*; Oxford University Press: New York, 1989.

(36) (a) Becke, A. D.; Density-Functional Thermochemistry, V. Systematic Optimization of Exchange-correlation Functional. *J. Chem. Phys.* **1997**, *107*, 8554–8560. (b) Hamprecht, F. A.; Cohen, A. J.; Tozer, D. J.; Handy, N. C. Development and Assessment of New Exchange-correlation Functional. *J. Chem. Phys.* **1998**, *109*, 6264–6272.

(37) Becke, A. D. Density-Functional Thermochemistry. III. The Role of Exact Exchange. *J. Chem. Phys.* **1993**, *98*, 5648–5652.

(38) Grimme, S. Semiempirical Hybrid Density Functional with Perturbative Second-order Correlation. *J. Chem. Phys.* **2006**, *124*, 034108–134123.

(39) Peterson, K. A.; Shepler, B. C.; Figgen, D.; Stoll, H. On the Spectroscopic and Thermochemical Properties of ClO, BrO, IO, and Their Anions. *J. Phys. Chem. A* **2006**, *110*, 13877–13883.

(40) Dunning, T. H., Jr. Gaussian Basis Sets for Use in Correlated Molecular Calculations. I. The Atoms Boron through Neon and Hydrogen. *J. Chem. Phys.* **1989**, *90*, 1007–1023.

(41) Woon, D. E.; Dunning, T. H., Jr. Gaussian Basis Sets for Use in Correlated Molecular Calculations. III. The Atoms Aluminum through Argon. *J. Chem. Phys.* **1993**, *98*, 1358–1371.

(42) Wadt, W. R.; Hay, P. J. Ab initio Effective Core Potentials for Molecular Calculations. Potentials for Main Group Elements Na to Bi. *J. Chem. Phys.* **1985**, *82*, 284–298.

(43) Weast, R. C. *CRC Handbook of Chemistry and Physics*, 65th ed.; CRC Press: Boca Raton, FL, 2003.

(44) Atkinson, R.; Baulch, D. L.; Cox, R. A.; Crowley, J. N.; Hampson, R. F.; Hynes, R. G.; Jenkins, M. E.; Rossi, M. J.; Troe, J. Evaluated Kinetic and Photochemical Data for Atmospheric Chemistry: Volume I - Gas Phase Reactions of Ox, HOx, NOx and SOx Species. *Atoms. Chem. Phys.* **2004**, No. 4, 1461–1783.

(45) Born, M.; Ingemann, S.; Nibbering, N. M. Heats of Formation of Mono-Halogen-Substituted Carbenes. Stability and Reactivity of  $\text{CHX}\bullet^-$  (X = F, Cl, Br, and I) Radical Anions. *J. Am. Chem. Soc.* **1994**, *116*, 7210–7217.

(46) NIST chemistry webbook, Oct 2012.

(47) Ellison, G. B.; Engelking, P. C.; Lineberger, W. C. An Experimental Determination of the Geometry and Electron Affinity of Methyl Radical. *J. Am. Chem. Soc.* **1978**, *100*, 2556–2558.

(48) (a) Sun, L.; Hase, W. L. Born-Oppenheimer Direct Dynamics Classical Trajectory Simulations. *Rev. Comput. Chem.* **2003**, *19*, 79–146. (b) Li, G.; Hase, W. L. Ab Initio Direct Dynamics Trajectory Study of the  $\text{Cl}^- + \text{CH}_3\text{Cl}$   $\text{S}_{\text{N}}2$  Reaction at High Reagent Translational Energy. *J. Am. Chem. Soc.* **1999**, *121*, 7124–7129.

(49) Hase, W. L.; Duchovic, R. J.; Hu, X.; Komornicki, A.; Lim, K. F.; Lu, D. H.; Peshlherbe, G. H.; Swamy, S. R.; Vande Linde, S. R.; Varandas, A.; et al. *QCPE Bull.* **1996**, *16*, 671.

(50) Hu, X.; Hase, W. L.; Pirraglia, T. Vectorization of the General Monte Carlo Classical Trajectory Program VENUS. *J. Comput. Chem.* **1991**, *12*, 1014–1024.

(51) Child, M. S. *Semiclassical Mechanics with Molecular Applications*; Oxford University Press: New York, 1991.

(52) Peshlherbe, G. H.; Wang, H.; Hase, W. L. Monte Carlo Sampling for Classical Trajectory Simulations. *Adv. Chem. Phys.* **1999**, *105*, 171–201.

(53) Schlier, C.; Seiter, A. Symplectic Integration of Classical Trajectories: A Case Study. *A. J. Phys. Chem. A* **1998**, *102*, 9399–9404.

(54) Schlier, C.; Seiter, A. High-Order Symplectic Integration: An Assessment. *Comput. Phys. Commun.* **2000**, *130*, 176–189.

(55) Eyring, H.; Walter, J. E.; Kimball, G. E. *Quantum Chemistry*; Wiley: New York, 1947.

(56) Hase, W. L.; Wolf, R. J.; Sloane, C. S. Trajectory Studies of the Molecular Dynamics of Ethyl Radical Decomposition. *J. Chem. Phys.* **1979**, *71*, 2911–2928.

(57) Morris, R. A.; Viggiano, A. A. Kinetics of the Reactions of  $\text{F}^-$  with  $\text{CF}_3\text{Br}$  and  $\text{CF}_3\text{I}$  as a Function of Temperature, Kinetic Energy, Internal Temperature, and Pressure. *J. Phys. Chem.* **1994**, *98*, 3740–3746.

(58) Cry, D. M.; Scarton, M. G.; Wiberg, K. B.; Johnson, M. A.; Nonose, S.; Hirokawa, J.; Tanaka, H.; Kondow, T.; Morris, R. A.; Viggiano, A. A. Observation of the  $\text{XY}^-$  Abstraction Products in the Ion–molecule Reactions  $\text{X}^- + \text{RY} \rightarrow \text{XY}^- + \text{R}$ : An Alternative to the  $\text{S}_{\text{N}}2$  Mechanism at Suprathermal Collision Energies. *J. Am. Chem. Soc.* **1995**, *117*, 1828–1832.

(59) Lowe, J. P. *Quantum Chemistry*; Academic Press: New York, 1978.

(60) Viggiano, A. A. Private communication.

(61) Mikosch, J.; Zhang, J.; Trippel, S.; Eichhorn, C.; Otto, R.; Sun, R.; de Jong, W. A.; Weidemüller, M.; Hase, W. L.; Wester, R. Indirect Dynamics in a Highly Exoergic Substitution Reaction. *J. Am. Chem. Soc.* **2013**, *135*, 4250–4259.

(62) Lourderaj, U.; Park, K.; Hase, W. L. Classical Trajectory Simulations of Post-Transition State Dynamics. *Int. Rev. Phys. Chem.* **2008**, *27*, 361–403.

(63) Hase, W. L.; Buckowski, D. G. Dynamics of Ethyl Radical Decomposition. II. Applicability of Classical Mechanics to Large Molecule Unimolecular Reaction Dynamics. *J. Comput. Chem.* **1982**, *3*, 335–343.

(64) Blanksby, S. J.; Ellison, G. B.; Bierbaum, V. M.; Kato, S. Direct Evidence for Base-Mediated Decomposition of Alkyl Hydroperoxides (ROOH) in the Gas Phase. *J. Am. Chem. Soc.* **2002**, *124*, 3196–3197.

(65) López, J. G.; Vayner, G.; Lourderaj, U.; Addepalli, S. V.; Kato, S.; de Jong, W. A.; Windus, T. L.; Hase, W. L. A Direct Dynamics Trajectory Study of  $\text{F}^- + \text{CH}_3\text{OOH}$  Reactive Collisions Reveals a Major Non-IRC Reaction Path. *J. Am. Chem. Soc.* **2007**, *129*, 9976–9985.